Fraunhofer
IWES

FRAUNHOFER-INSTITUT FOR WIND ENERGY AND ENERGY SYSTEM TECHNOLOGY IWES

IWES WIND TURBINE IWT-7.5-164 REV. 2.5

21.06.2017

Contact

Fraunhofer Institute for Wind Energy und Energy System Technology IWES Northwest
Am Seedeich 45
27572 Bremerhaven
Germany

Phone: +49 (0) 471 14290-100
E-Mail: iweswindturbine@iwes.fraunhofer.de
www.windenergie.iwes.fraunhofer.de

Change log				
IWT Revision	Version	**Issue date**	**Authors**	**Change**
0	00	30.12.2013	Alper Sevin[1], Malo Rosemeier[1], Moritz Bätge[1], Roman Braun[1], Fanzhong Meng[1], Martin Shan[1], Daria Horte[2], Claudio Balzani[2], Andreas Reuter[1]	Initial document
1	00	11.08.2014	Alper Sevin[1], Malo Rosemeier[1], Moritz Bätge[1], Roman Braun[1], Fanzhong Meng[1], Martin Shan[1], Daria Horte[2], Claudio Balzani[2], Andreas Reuter[1]	Controller update, blade design update
2	00	11.03.2015	Alper Sevin[1], Malo Rosemeier[1], Moritz Bätge[1], Roman Braun[1], Fanzhong Meng[1], Martin Shan[1], Daria Horte[2], Claudio Balzani[2], Andreas Reuter[1]	Included controller specification, new structural blade data
2.5	00	15.08.2016	Oliver Bleich[1], Fanzhong Meng[1], Elia Daniele[1], Philipp Thomas[1], Wojciech Popko[1]	- Corrected hub mass, nacelle mass, and blade mass according to BECAS HAWC2 output - add Acknowledgements - add Nomenclature - add list of figures - add list of tables - add coordinate system description - updated each figure with updated simulation model - enhanced image quality - updated Campbell diagram with updated simulation model and included more eigenfrequencies for rotor blades and tower - add visualization of eigenforms - add drawing of nacelle geometry - enhanced the description of the turbine controller - enhance control parameter tuning and step response curves - add power production simulation time series - enhance IPC parameter tuning description - add original airfoil data for an aoa range of -180° to 180° - add blended airfoil data for an aoa range of -180° to 180° at 31 stations along the rotor blade
2.5	01	21.06.2017	Philipp Thomas[1]	Change Acknowledgements, Authors and change log

[1]Fraunhofer Institute for Wind Energy and Energy System Technologie IWES Northwest, Am Seedeich 45, 27572 Bremerhaven
[2]Leibnitz Universität Hannover – Institute of Wind Energy Systems, Appelstraße 9A, 30167 Hannover

Content

Acknowledgements

The present work was funded within the framework of the joint project Smart Blades (0325601A/B/C/D) by the German Federal Ministry for Economic Affairs and Energy (BMWi) under decision of the German Federal Parliament.

Nomenclature

Abbreviation	Description
BECAS	Beam Cross section Analysis Software
BEM	Blade Element Momentum
DTU	Danmarks Tekniske Universitet
HAWC2	Horizontal Axis Wind turbine simulation Code 2nd generation
IEC	International Electrotechnical Commission
NREL	National Renewable Energy Laboratory
NTM	Normal Turbulence Model
PID	Proportional-Integral-Derivative
RFOIL	Radial XFOIL
XFOIL	Subsonic Airfoil Development System

Symbol	Description
A	Cross sectional area
A_{blade}	Blade surface area
$C_{1/2}$	Blade half chord position
CG_{hub}	Center of gravity of the hub
$CG_{generator}$	Center of gravity of the generator
$CG_{nacelle}$	Center of gravity of the nacelle
D_{rotor}	Rotor diameter (unconed)
D_{tower}	Tower outside diameter
E	Young's modulus
G	Shear modulus
I_x	Area moment of inertia with respect to principal bending x_e axis. This is the principal bending axis most parallel to the x_{c2} axis
I_y	Area moment of inertia with respect to principal bending y_e axis
K	Torsional stiffness constant with respect to z_e axis at the shear center. For a circular section only this is identical to the polar moment of inertia
K_1	Linear gain scheduling factor
K_2	Quadratic gain scheduling factor
K_{opt}	Optimal generator constant
L_d	Transformed load d-component in the non-rotating reference frame
L_i	Three blade loads in the rotating reference frame ($i = 1, 2, 3$)
L_q	Transformed load q-component in the non-rotating reference frame
$P_{r,k}$	generator power set-point at time step k
Q_A	Aerodynamic torque
$Q_{max,k}$	Maximum generator torque limit at time step k
$Q_{min,k}$	Minimum generator torque limit at time step k
$Q_{ref,k}$	Demanded generator torque at time step k
S_F	Safety factor
$S_{\theta,k}$	Switch value interpolated by Spline function at each time step (zero is partial load region; one is full load region)
V_{in}	Cut-in wind speed

V_{out}	Cut-out wind speed
V_r	Rated wind speed
V_{tip_r}	Rated tip speed
c	Blade chord length
h_{hub}	Hub height
k	Time step
k_x	Shear factor for force in principal bending x_e direction
k_y	Shear factor for force in principal bending y_e direction
l_{blade}	Rotor blade length
m	Mass per unit length
m_{RNA}	Rotor-Nacelle-Assembly mass
m_{blade}	Total blade mass
m_{tower}	Tower mass
r	Curved length distance from blade root along center line
r_{ix}	Radius of gyration related to elastic center. Corresponds to rotation about principal bending axis x_e
r_{iy}	Radius of gyration related to elastic center. Corresponds to rotation about principal bending axis y_e
t	Blade thickness
t_{tower}	Tower wall thickness
x_h	Hub x-coordinate
x_b	Local blade x-coordinate
x_e	x_{c2} coordinate from $C_{1/2}$ to center of elasticity. The elastic center is the point where radial force (in the z-direction) does not contribute to bending around the x or y directions
x_m	x_{c2} coordinate from $C_{1/2}$ to mass center
x_{pa}	Distance from leading edge to pitch axis divided by chord length
x_s	Shaft x-coordinate
x_s	x_{c2} coordinate from $C_{1/2}$ to shear center. The shear center is the point where external forces only contribute to pure bending and no torsion
x_t	Tower x-coordinate
x_{tt}	Tower top x-coordinate
y_h	Hub y-coordinate
y_b	Local blade y-coordinate
y_b	Pre-bending in flap-wise direction measured from the pitch axis
y_e	y_{c2} coordinate from $C_{1/2}$ to center of elasticity. The elastic center is the point where radial force (in the z-direction) does not contribute to bending around the x or y directions
y_m	y_{c2} coordinate from $C_{1/2}$ to mass center
y_s	Shaft y-coordinate
y_s	y_{c2} coordinate from $C_{1/2}$ to shear center. The shear center is the point where external forces only contribute to pure bending and no torsion
y_t	Tower y-coordinate
y_{tot_b}	Total blade pre-bending
y_{tt}	Tower top y-coordinate
z_h	Hub z-coordinate
z_b	Local blade z-coordinate
z_s	Shaft z-coordinate
z_t	Tower z-coordinate

z_{tt}	Tower top z-coordinate
Ω_k	Current rotor speed at time step k
$\overline{\Omega}_k$	Filtered rotor speed at time step k
Ω_{min0}	Interpolation rotor speed limits used for calculate $\sigma_{min,k}$
Ω_{min1}	Interpolation rotor speed limits used for calculate $\sigma_{min,k}$
Ω_{max0}	Interpolation rotor speed limits used for calculate $\sigma_{max,k}$
Ω_{max1}	Interpolation rotor speed limits used for calculate $\sigma_{max,k}$
Ω_{min}	Minimum rotational speed when the generator is put online
$\Omega_{r,k}$	Rotor speed set-point at time step k
α	Thermal expansion coefficient
ζ_0	Damping ratio of the filter
η_{tot}	Total turbine efficiency
λ_D	Design tip speed ratio
θ	Collective pitch angle
$\theta_{I,k}$	Integral term of demanded collective pitch angle at time step k
$\theta_{P,k}$	Proportional term of demanded collective pitch angle at time step k
θ_{cone}	Blade cone angle (upwind)
$\theta_{d,k}$	Derivative term of demanded collective pitch angle at time step k
$\theta_{min,k}$	Minimum limit of demanded collective pitch angle at time step k
$\theta_{ref,k}$	Demanded collective pitch angle at time step k
θ_{s1}	Low angle limits in between switches to full load
θ_{s2}	High angle limits in between switches to full load
θ_{struct}	Structural pitch about z_{c2} axis. This is the angle between the x_{c2} axis and the main principal bending axis x_e.
θ_{tilt}	Shaft tilt angle (upwards from horizon)
θ_{twist}	Blade twist angle
ρ	Material density
$\sigma_{max,k}$	Maximum limit of interpolation factor at time step k
$\sigma_{min,k}$	Minimum limit of interpolation factor at time step k
τ	Time constant of the filter
φ	Rotor azimuth angle
ψ_{rotor}	Specific power (per swept area)
ω_0	Frequency of the filter

List of figures

List of tables

1 Introduction

Detailed wind turbine models for load simulations are essential for many research topics as they build the base for the verification and validation of most of the different disciplines in wind energy research. Turbine models, for instance the NREL 5-MW Offshore Baseline Turbine [1] or the DTU 10MW turbine [2], were developed in the last years and are used to contribute to wind turbine research especially in terms of further development of turbine design, controller and engineering methods on wind turbines. However, the turbine models that have been developed until now are not competitive with current industry turbines in terms of design requirements and control strategies. That is why the comparability between research and manufactured turbines is diverging.

A new state-of-the-art 7.5 MW turbine model was designed within the Smart Blades project funded by the Federal Ministry for Economic Affairs and Energy[1]. This turbine model has a specific design focus on rotor blades and tower structure. The turbine design has been adapted based on results from fatigue and extreme loads simulation according to IEC61400-1 Ed.3 [3]. The implementation of several controller features such as peak-shaver and individual pitch control was an important aspect of the design. Many of these modifications were already developed and implemented in industry turbines but need further investigation for scientific purposes. This specification includes technical data to implement the numerical turbine model in a simulation environment and serves as a baseline for detailed component design and scientific research.

[1] http://www.bmwi.de

2
Coordinate systems

The coordinate system for the description of the turbine design in chapter 3 can be seen in Figure 2-1. The tower coordinate system is denoted by x_t, y_t, z_t, the tower top coordinate system by x_{tt}, y_{tt}, z_{tt}, the shaft coordinate system by x_s, y_s, z_s, the hub coordinate system by x_h, y_h, z_h and the local blade coordinate system by x_b, y_b, z_b.

The hub coordinate system rotates with the rotor and has its origin at the center of the blade root. The z-axis points towards the blade tip along the pitch axis, the y-axis is perpendicular to the x-axis and points downwind. The x-axis creates the right hand Cartesian coordinate system.

The local blade coordinate system is a right hand Cartesian coordinate system and rotates with the rotor and pitches with the blade. It has its origin at the half chord position of each blade section and follows the blade center line position and orientation. The x-axis points towards edgewise direction and the y-axis towards the flapwise direction.

The y-axis of the tower coordinate system points down wind with respect to the main wind direction. The negative z-axis points upwards. The x-axis forms a right hand Cartesian coordinate system. The origin is at the tower bottom at the centerline of the tower.

The y-axis of the tower top coordinate system points down wind with respect to the main wind direction. The negative z-axis points upwards. The x-axis forms a right hand Cartesian coordinate system. The origin is at the tower top.

The z-axis of the shaft coordinate system points up wind with respect to the main wind direction. It is rotated positive (upwards with respect to the horizon) about the shaft tilt angle θ_{tilt}. The y-axis is perpendicular to the z-axis and points downwards to the ground. The x-axis forms a right hand system. The origin is located vertically above the tower coordinate system at the center line of the shaft.

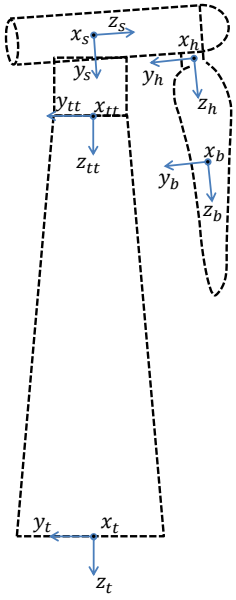

Figure 2-1: Coordinate systems

3
Wind turbine

The goal was to design a large state-of-the-art onshore turbine with a relatively low rated power per swept area, a direct drive generator and a load-optimized control strategy and blade design. In order to facilitate comparability with industry turbines the IWES Wind Turbine IWT-7.5-164 is designed according to the wind class IEC A1 [3]. Although sites with wind class A1 are rare, these conditions have been chosen to include "worst case" scenarios in terms of turbulence and extreme wind speeds.

3.1
Main design parameters

Table 3-1 summarizes the main parameters of the IWT-7.5-164.

Table 3-1: Main turbine parameters

Rated generator power	P_r	7.5 MW
Wind class		IEC A1
Hub height	h_{hub}	119.3 m
Rotor diameter (unconed)	D_{rotor}	164 m
Rotor blade length (along pitch axis)	l_{blade}	80 m
Specific power (per swept area)	ψ_{rotor}	355 W/m²
Cut-in wind speed	V_{in}	3 m/s
Rated wind speed	V	11 m/s
Cut-out wind speed	V_{out}	25 m/s
Minimum rotational speed	Ω_{min}	5 rpm
Rated rotational speed	Ω_r	10 rpm
Rated tip speed	V_{tip_r}	85.9 m/s
Design tip speed ratio	λ_D	8.4
Blade cone angle (upwind)	θ_{cone}	2 °
Shaft tilt angle (upwards from horizon)	θ_{tilt}	5 °
Total turbine efficiency	η_{tot}	95%
Drive train concept		Direct drive
Control concept		Variable speed, individual pitch-control, peak-shaver
Rotor configuration		Upwind, 3-blade
Tower mass	m_{tower}	1467355 kg
Rotor-Nacelle-Assembly mass	m_{RNA}	536586 kg

3.2 Steady state performance

The power curve and the pitch angle curve are shown in Figure 3-1 and Figure 3-2, respectively. Figure 3-3 shows the torque-speed curve. All results are derived from steady state simulations with BEM.

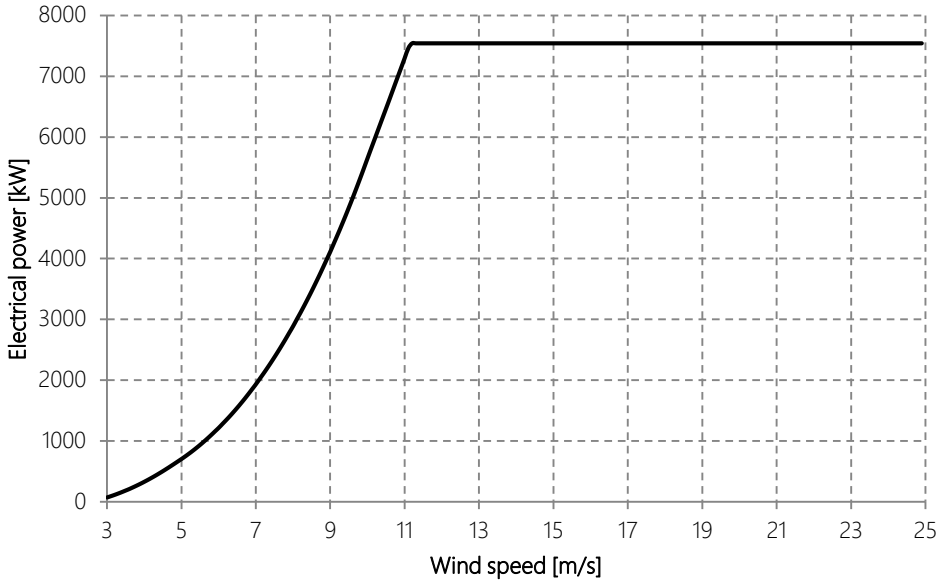

Figure 3-1: Power curve

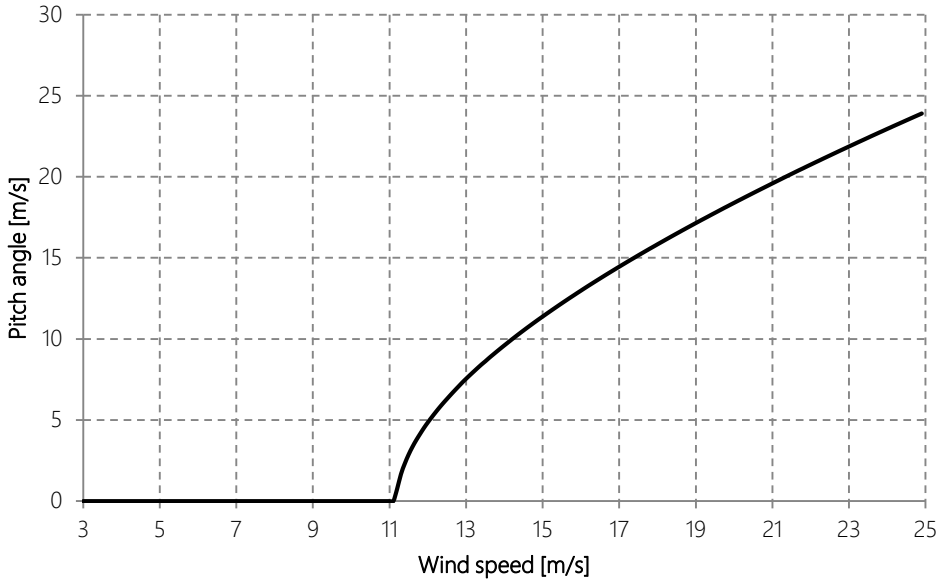

Figure 3-2: Pitch curve

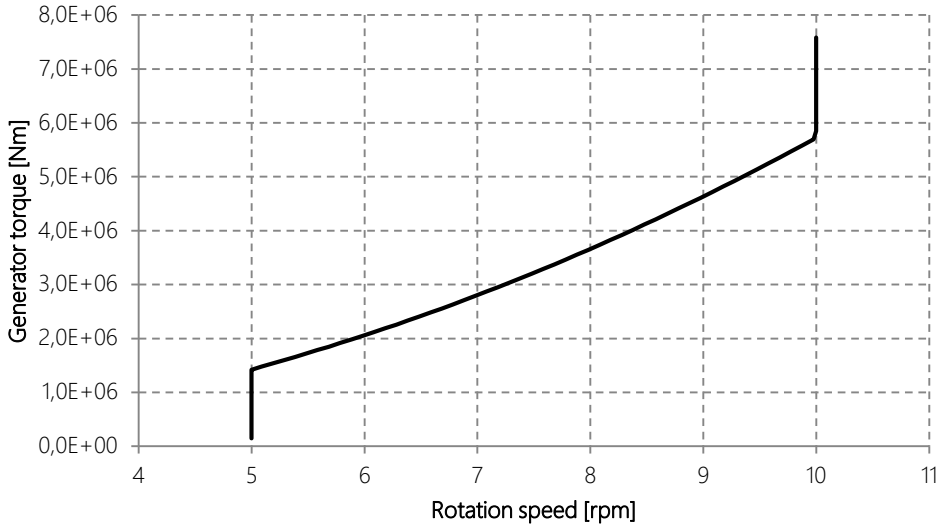

Figure 3-3: Torque-speed curve

3.3 Tower

For the tower design a soft-stiff hybrid tower (concrete/steel) with a hub height of 120 m and a first eigenfrequency of 0.254 Hz which fits between the 1P- and the 3P-excitation is used. This design has the advantage that the stiffness of the lower part is very high; and therefore comparable with offshore support structures.
This approach was also successfully used for the Multibrid M5000 prototype [4]. The large rotor diameter contributes to a high thrust, which leads to high bending moment at the tower bottom. Therefore, a large tower diameter is required as otherwise the fatigue loads would exceed the tower strength.

3.3.1 Tower structural parameters

The used materials and the detailed tower design are given in Table 3-2 and Table 3-3. The structure is cantilevered at the bottom where 6 DOFs are constrained. An influence from different soil characteristics can cause variations of the system eigenfrequency and damping.

Table 3-2: Tower material data

	Young's modulus E	Shear modulus G	Density ρ	Thermal expansion coefficient α	Safety factor S_F
Material	N/m²	N/m²	kg/m³	1/°C	-
Construction steel S355	2.10E+11	8.10E+10	7850	1.20E-05	1.1
Concrete C50/60	3.43E+10	1.43E+10	2500	1.00E-05	1.0

Table 3-3: Tower structural properties

	Height	Outer diameter D_{tower}	Wall thickness t_{tower}	Material	Mass per unit length	Bending stiffness	Shear stiffness	Torsional stiffness	Axial stiffness
Section	m	m	mm	-	kg/m	Nm²	N	Nm²	N
1	0	8.40	450	concrete	2.81E+04	3.06E+12	8.04E+10	2.55E+12	3.86E+11
	22	6.70	450	concrete	2.21E+04	1.49E+12	6.32E+10	1.24E+12	3.03E+11
2	22	6.70	400	concrete	1.98E+04	1.35E+12	5.66E+10	1.13E+12	2.72E+11
	36	5.62	400	concrete	1.64E+04	7.71E+11	4.69E+10	6.43E+11	2.25E+11
3	36	5.62	350	concrete	1.45E+04	6.93E+11	4.14E+10	5.78E+11	1.99E+11
	49	5.62	350	concrete	1.45E+04	6.93E+11	4.14E+10	5.78E+11	1.99E+11
4	49	5.62	350	concrete	1.45E+04	6.93E+11	4.14E+10	5.78E+11	1.99E+11
	64	5.62	350	concrete	1.45E+04	6.93E+11	4.14E+10	5.78E+11	1.99E+11
5	64	5.62	700	concrete	2.70E+04	1.15E+12	7.74E+10	9.55E+11	3.71E+11
	66	4.62	700	concrete	2.16E+04	5.86E+11	6.16E+10	4.89E+11	2.96E+11
6	66	4.30	57	steel	5.96E+03	3.59E+11	3.08E+10	2.77E+11	1.60E+11
	70	4.30	57	steel	5.96E+03	3.59E+11	3.08E+10	2.77E+11	1.60E+11
7	70	4.30	45	steel	4.72E+03	2.86E+11	2.44E+10	2.21E+11	1.26E+11
	87	3.99	45	steel	4.38E+03	2.28E+11	2.26E+10	1.76E+11	1.17E+11
8	87	3.99	43	steel	4.19E+03	2.18E+11	2.16E+10	1.69E+11	1.12E+11
	105	3.38	43	steel	3.53E+03	1.31E+11	1.82E+10	1.01E+11	9.46E+10
9	105	3.38	30	steel	2.48E+03	9.27E+10	1.28E+10	7.15E+10	6.62E+10
	116	3.00	30	steel	2.20E+03	6.48E+10	1.13E+10	5.00E+10	5.88E+10

3.4 Rotor blade

In this Section the structural (see Section 3.4.2) and the aerodynamic (see Section 3.4.3) design of the blade is described. Parameters for the design are listed in Table 3-4. Pre-bending in the flapwise direction is applied to increase the tower clearance.

Table 3-4: General blade parameters

Blade length (along pitch axis)	l_{blade}	80 m
Total blade mass	m_{blade}	30862 kg
Blade surface	A_{blade}	646.65 m²
Design tip speed ratio	λ_D	8.4
Total blade pre-bending	y_{tot_b}	4.5 m

3.4.1 Dimensionless performance curves

The aerodynamic coefficients for power, thrust and torque are determined with the BEM theory and presented in Figure 3-4 to Figure 3-6.

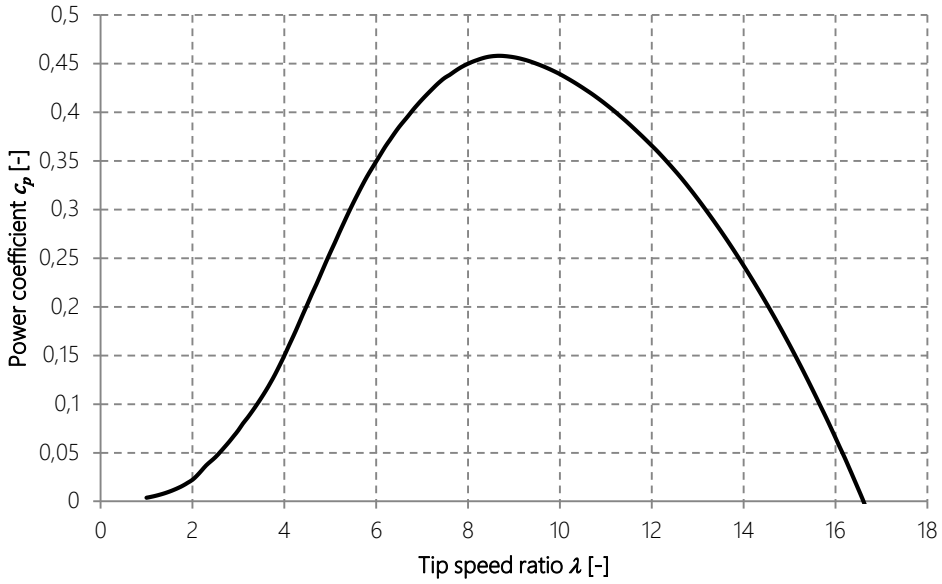

Figure 3-4: Power coefficient C_p versus tip speed ratio λ

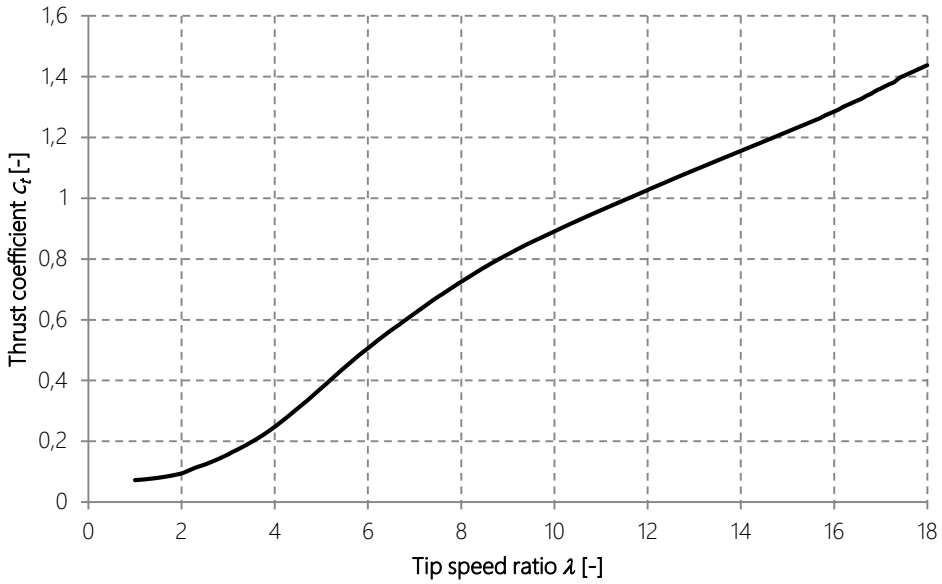

Figure 3-5: Thrust coefficient C_t versus tip speed ratio λ

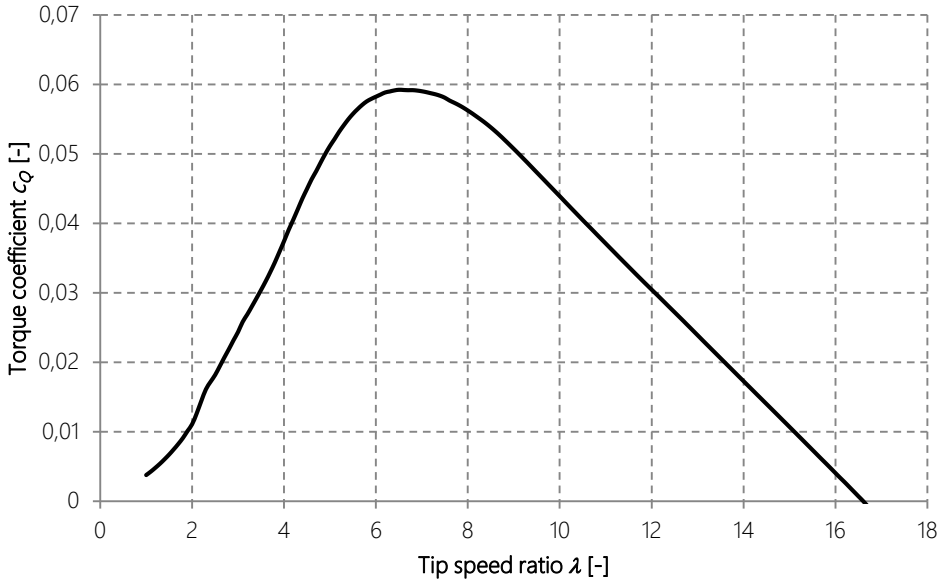

Figure 3-6: Torque coefficient C_Q versus tip speed ratio λ

3.4.2 Structural design

The structural parameters were calculated at design specific positions over the blade span (see Table 3-6). The positions for the different centers are defined by the half chord length position $C_{1/2}$(see Figure 3-7).

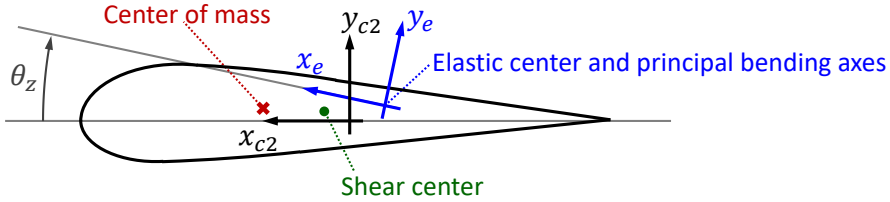

Figure 3-7: Position of structural centers related half chord coordinate system ($c2$) [5]

Table 3-5 provides the description of the used variables. The values presented in Table 3-6 were derived with BECAS [6] according to the manual for the structural data in HAWC2 [5].

Table 3-5: Description of structural variables

Variable	Unit	Description
r	m	Curved length distance from blade root along center line
m	kg/m	Mass per unit length
x_m	m	x_{c2} coordinate from $C_{1/2}$ to mass center
y_m	m	y_{c2} coordinate from $C_{1/2}$ to mass center
r_{ix}	m	Radius of gyration related to elastic center. Corresponds to rotation about principal bending axis x_e
r_{iy}	m	Radius of gyration related to elastic center. Corresponds to rotation about principal bending axis y_e
x_s	m	x_{c2} coordinate from $C_{1/2}$ to shear center. The shear center is the point where external forces only contribute to pure bending and no torsion.
y_s	m	y_{c2} coordinate from $C_{1/2}$ to shear center. The shear center is the point where external forces only contribute to pure bending and no torsion.
E	N/m²	Young's modulus
G	N/m²	Shear modulus
I_x	m^4	Area moment of inertia with respect to principal bending x_e axis. This is the principal bending axis most parallel to the x_{c2} axis
I_y	m^4	Area moment of inertia with respect to principal bending y_e axis
K	m^4/rad	Torsional stiffness constant with respect to z_e axis at the shear center. For a circular section only this is identical to the polar moment of inertia.
k_x	-	Shear factor for force in principal bending x_e direction
k_y	-	Shear factor for force in principal bending y_e direction
A	m²	Cross sectional area
θ_{struct}	deg	Structural pitch about z_{c2} axis. This is the angle between the x_{c2} axis and the main principal bending axis x_e.
x_e	m	x_{c2} coordinate from $C_{1/2}$ to center of elasticity. The elastic center is the point where radial force (in the z-direction) does not contribute to bending around the x or y directions.
y_e	m	y_{c2} coordinate from $C_{1/2}$ to center of elasticity. The elastic center is the point where radial force (in the z-direction) does not contribute to bending around the x or y directions.

Table 3-6: Blade properties

r	m	x_m	y_m	r_{ix}	r_{iy}	x_s	y_s	E	G	I_x	I_y	K	k_x	k_y	A	θ_{twist}	x_e	y_e
m	kg/m	m	m	m	m	m	m	N/m²	N/m²	m⁴	m⁴	m⁴/rad	-	-	m²	deg	m	m
0.00	2990.99	0.00	0.00	1.37	1.37	0.00	0.00	2.53E+10	8.10E+09	2.99	2.99	5.98	0.50	0.50	1.60	-3.31	0.00	0.00
2.00	2059.98	0.01	0.00	1.38	1.38	0.00	0.00	2.45E+10	7.85E+09	2.21	2.15	4.35	0.50	0.50	1.14	19.99	0.01	0.00
4.00	956.84	0.07	0.01	1.37	1.38	0.01	0.01	1.05E+10	3.70E+09	2.20	1.98	3.81	0.47	0.50	1.05	30.67	0.07	0.00
6.00	834.08	-0.16	-0.01	1.38	1.45	-0.05	0.00	9.30E+09	3.23E+09	2.04	2.25	3.77	0.50	0.47	1.02	-19.02	-0.16	0.00
8.00	773.86	-0.35	-0.03	1.30	1.59	-0.08	-0.05	8.44E+09	2.81E+09	1.99	2.62	3.67	0.51	0.42	1.05	-19.86	-0.28	-0.03
10.00	713.75	-0.48	-0.04	1.20	1.72	-0.22	-0.15	8.43E+09	2.64E+09	1.72	2.73	3.33	0.53	0.40	1.01	-12.28	-0.38	-0.04
12.00	634.42	-0.55	-0.03	1.11	1.77	-0.11	-0.09	8.52E+09	2.48E+09	1.41	2.51	2.56	0.53	0.36	0.93	-10.18	-0.42	-0.04
14.00	598.83	-0.58	-0.02	1.02	1.75	-0.02	-0.08	9.25E+09	2.51E+09	1.14	2.16	1.98	0.54	0.33	0.86	-8.81	-0.42	-0.03
16.00	561.08	-0.60	-0.01	0.93	1.69	-0.01	-0.06	1.01E+10	2.58E+09	0.89	1.77	1.51	0.55	0.31	0.79	-7.59	-0.42	-0.03
18.00	512.77	-0.60	-0.01	0.84	1.61	-0.05	-0.06	1.09E+10	2.61E+09	0.67	1.37	1.15	0.54	0.30	0.71	-6.92	-0.39	-0.02
21.00	444.19	-0.59	0.00	0.74	1.49	-0.03	-0.05	1.25E+10	2.63E+09	0.45	0.94	0.75	0.56	0.25	0.61	-5.85	-0.35	-0.02
25.00	415.18	-0.62	0.03	0.61	1.34	-0.11	0.08	1.47E+10	2.91E+09	0.27	0.63	0.43	0.55	0.21	0.53	-5.30	-0.34	-0.01
27.00	391.85	-0.59	0.03	0.56	1.26	-0.09	0.07	1.59E+10	2.95E+09	0.21	0.50	0.33	0.54	0.20	0.49	-4.70	-0.31	-0.01
29.00	365.66	-0.54	0.03	0.51	1.18	0.07	0.06	1.78E+10	3.06E+09	0.16	0.39	0.23	0.53	0.17	0.45	-4.10	-0.28	-0.01
31.00	352.03	-0.54	0.02	0.47	1.14	0.02	0.07	1.90E+10	3.12E+09	0.13	0.34	0.18	0.53	0.17	0.42	-3.26	-0.28	-0.01
35.00	313.80	-0.51	0.03	0.41	1.04	0.03	0.08	2.05E+10	3.10E+09	0.09	0.25	0.12	0.51	0.16	0.37	-2.44	-0.26	0.00
39.00	271.47	-0.47	0.02	0.36	0.96	0.02	0.08	2.21E+10	3.12E+09	0.06	0.18	0.08	0.50	0.15	0.33	-2.09	-0.23	0.00
43.00	241.90	-0.45	0.03	0.32	0.89	0.01	0.08	2.27E+10	3.14E+09	0.04	0.14	0.05	0.50	0.14	0.29	-1.87	-0.23	0.01
47.00	214.62	-0.43	0.03	0.28	0.83	0.03	0.10	2.27E+10	3.21E+09	0.03	0.11	0.04	0.53	0.13	0.25	-1.87	-0.23	0.01
51.00	191.25	-0.41	0.03	0.24	0.78	0.02	0.09	2.19E+10	3.20E+09	0.02	0.08	0.03	0.54	0.13	0.23	-1.96	-0.23	0.01
55.00	159.46	-0.35	0.02	0.22	0.71	0.05	0.04	2.09E+10	2.85E+09	0.01	0.06	0.02	0.49	0.13	0.20	-1.64	-0.22	0.01
59.00	133.43	-0.32	0.03	0.19	0.65	0.05	0.04	1.98E+10	2.96E+09	0.01	0.05	0.01	0.50	0.13	0.17	-1.68	-0.21	0.01
63.00	107.89	-0.29	0.03	0.17	0.60	0.04	0.04	1.93E+10	3.01E+09	0.01	0.03	0.01	0.52	0.13	0.13	-1.37	-0.19	0.02
67.00	79.99	-0.24	0.03	0.15	0.54	0.03	0.04	1.76E+10	2.82E+09	0.00	0.02	0.00	0.54	0.15	0.10	-1.03	-0.16	0.03
69.00	67.66	-0.21	0.03	0.14	0.50	0.02	0.04	1.65E+10	2.81E+09	0.00	0.01	0.00	0.56	0.15	0.09	-0.75	-0.14	0.03
71.00	58.52	-0.19	0.03	0.13	0.47	0.02	0.05	1.60E+10	2.86E+09	0.00	0.01	0.00	0.58	0.15	0.08	-0.67	-0.13	0.03
73.00	51.63	-0.17	0.03	0.11	0.43	0.02	0.05	1.55E+10	3.00E+09	0.00	0.01	0.00	0.57	0.15	0.06	-0.55	-0.13	0.03
74.00	48.17	-0.16	0.03	0.10	0.41	0.01	0.05	1.56E+10	3.10E+09	0.00	0.01	0.00	0.57	0.15	0.06	-0.48	-0.13	0.03
76.00	38.16	-0.13	0.03	0.09	0.35	0.00	0.04	1.59E+10	3.25E+09	0.00	0.00	0.00	0.55	0.15	0.04	-0.46	-0.11	0.03
78.00	26.27	-0.09	0.02	0.06	0.26	0.00	0.03	1.88E+10	3.98E+09	0.00	0.00	0.00	0.56	0.14	0.03	-0.68	-0.09	0.02
79.98	0.26	-0.05	0.02	0.03	0.16	-0.02	0.02	2.23E+10	4.70E+09	0.00	0.00	0.00	0.55	0.13	0.00	-0.82	-0.06	0.02

3.4.3
Aerodynamic design

The airfoils developed by the TU Delft [7], [8] and by Fraunhofer IWES were used for the aerodynamic design. The relative thickness of the original airfoils and their span-wise locations are given in Table 3-7. The discretization of the entire blade geometry is achieved by the generation of several linear interpolated airfoil shapes in between the original ones, introducing so-called "blended" airfoils based on the relative distance of the considered station from the neighbor original airfoils. In Table 3-8 the entire blade geometry is reported. The distributions of the blade relative thickness, chord length and twist angle are shown in Figure 3-8, Figure 3-9 and Figure 3-10, respectively. The aerodynamic parameters of the original and the interpolated airfoils are available in Appendix A and Appendix B, respectively. The following symbols are used in Table 3-8:

- Span-wise coordinate z.
- Relative thickness t/c , i.e. the absolute thickness divided by chord length (see Figure 3-8).
- Chord length c (see Figure 3-9).
- Twist angle θ_{twist} (see Figure 3-10).
- Distance from leading edge to pitch axis divided by chord length x_{pa}.
- Pre-bending in flap-wise direction y_b measured from the pitch axis.

Table 3-7: Relative thickness and span-wise position of the original profiles

	Rel. thickness t/c	**Span-wise coordinate z**
Airfoil	-	m
Circle	1.00	0.00
IWES-A1 600-180	0.60	10.33
IWES-A1 500-100	0.50	13.76
IWES-A1 400-050	0.40	24.25
DU 00-W2-350	0.35	34.80
DU 91-W2-250	0.25	58.60
DU 08-W-210-6.5	0.21	70.47
DU 08-W-180-6.5	0.18	79.98

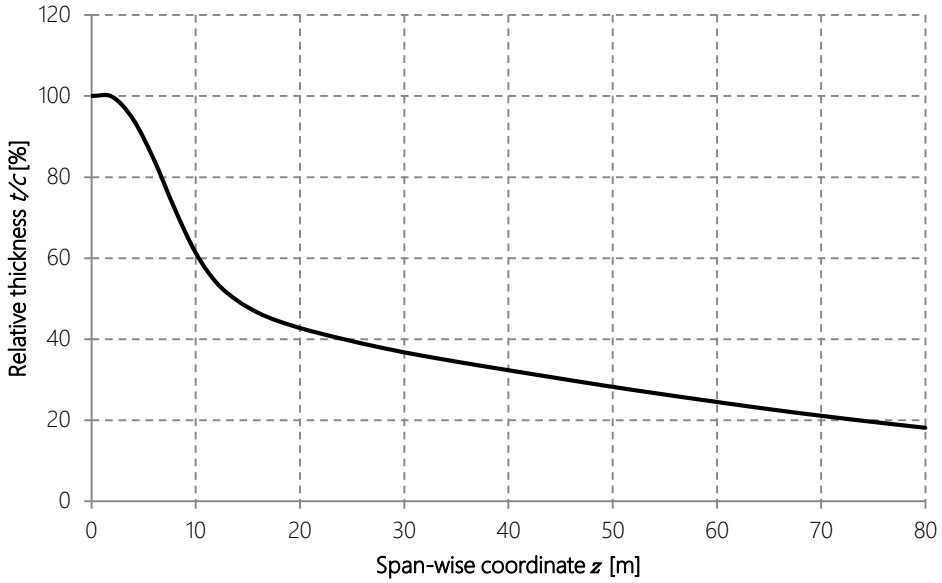

Figure 3-8: Relative thickness over blade length

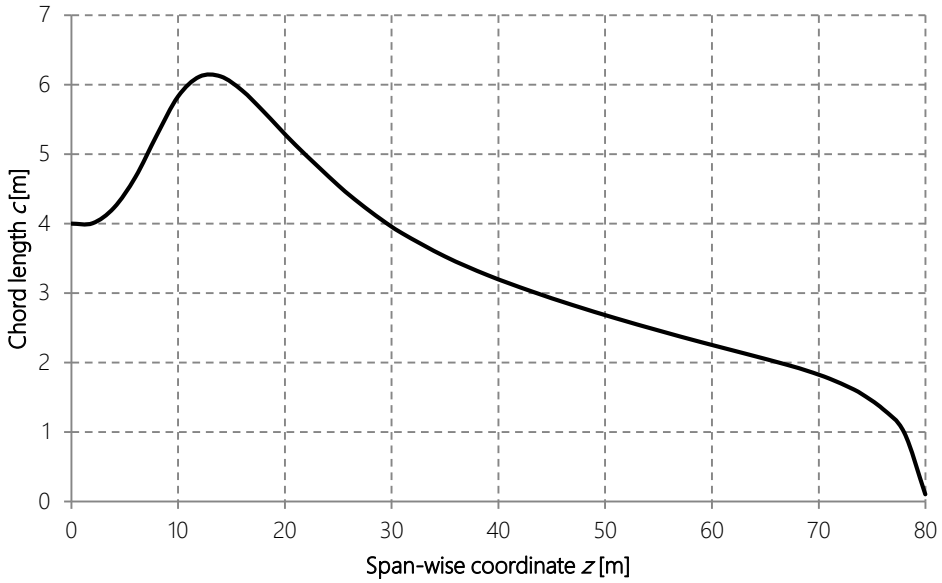

Figure 3-9: Chord length over blade length

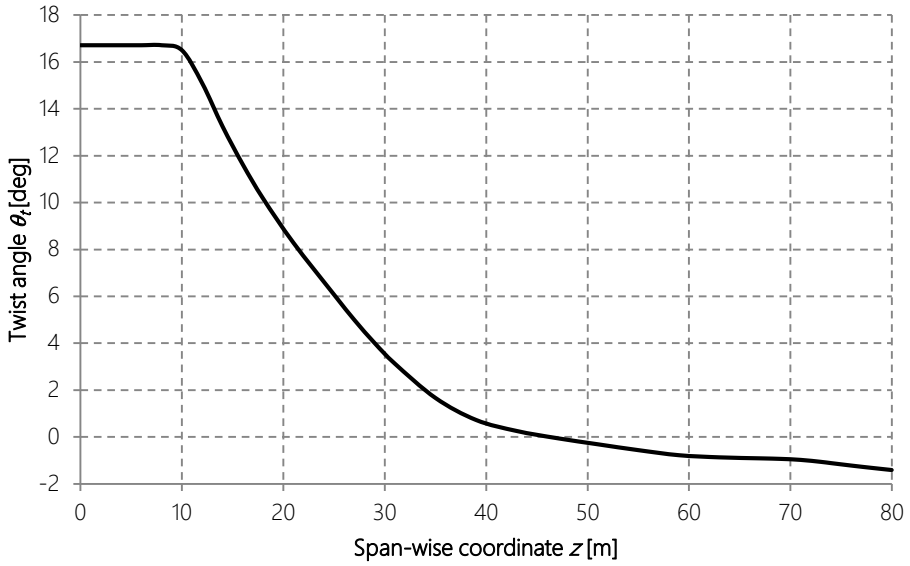

Figure 3-10: Twist angle over blade length

Table 3-8: Aerodynamic blade geometry

	z	c	θ_{twist}	t/c	x_{pa}	y_b
Station	m	m	deg	%	%	m
1	0.00	4.000	16.709	100.000	50.000	0.000
2	2.00	4.006	16.709	99.790	49.985	0.000
3	4.00	4.229	16.709	94.231	48.406	0.000
4	6.00	4.668	16.709	84.271	45.016	0.000
5	8.00	5.270	16.709	72.098	41.125	0.000
6	10.00	5.830	16.494	61.323	38.355	-0.001
7	12.00	6.115	15.085	53.934	36.765	-0.001
8	14.00	6.118	13.246	49.533	35.791	-0.003
9	16.00	5.916	11.62	46.525	35.107	-0.007
10	18.00	5.615	10.167	44.417	34.582	-0.012
11	21.00	5.132	8.276	42.068	33.939	-0.026
12	25.00	4.551	6.067	39.538	33.222	-0.057
13	27.00	4.294	4.990	38.383	32.923	-0.079
14	29.00	4.063	4.003	37.305	32.661	-0.107
15	31.00	3.860	3.122	36.304	32.432	-0.141
16	35.00	3.527	1.661	34.488	32.059	-0.229
17	39.00	3.258	0.723	32.792	31.774	-0.349
18	43.00	3.031	0.254	31.126	31.545	-0.505
19	47.00	2.826	-0.054	29.475	31.352	-0.702
20	51.00	2.638	-0.314	27.883	31.181	-0.946
21	55.00	2.462	-0.564	26.370	31.023	-1.239
22	59.00	2.294	-0.78	24.909	30.871	-1.589
23	63.00	2.134	-0.871	23.469	30.719	-1.998
24	67.00	1.970	-0.914	22.105	30.564	-2.473
25	69.00	1.878	-0.936	21.460	30.485	-2.735
26	71.00	1.770	-0.979	20.834	30.404	-3.013
27	73.00	1.634	-1.064	20.218	30.320	-3.312
28	74.00	1.551	-1.117	19.916	30.277	-3.469
29	76.00	1.333	-1.222	19.325	30.189	-3.797
30	78.00	0.995	-1.320	18.748	30.096	-4.138
31	79.98	0.105	-1.412	18.190	30.000	-4.500

3.5 Eigenfrequencies and Campbell diagram

Possible resonant vibrations of the entire turbine resulting from interaction with the spinning rotor are identified in the Campbell diagram in Figure 3-11, where system frequencies are plotted versus the rotational speed of the rotor. The Campbell diagram shows the linear excitation lines (up to 9P) of the 3-bladed rotor in the operational rotation speed range between 5 and 10 rpm. All shown modes are coupled and the whole system is considered. The tower eigenfrequency fits between the 1P- and the 3P-excitation (except for the region very close to the minimum rotational speed of 5 rpm). Simulation for the region around 5 rpm showed that the aerodynamic and structural damping will damp out possible excitations. Figure 3-12 to Figure 3-20 show the shapes of the main modes. Note that the blade modes presented in these figure are uncoupled.

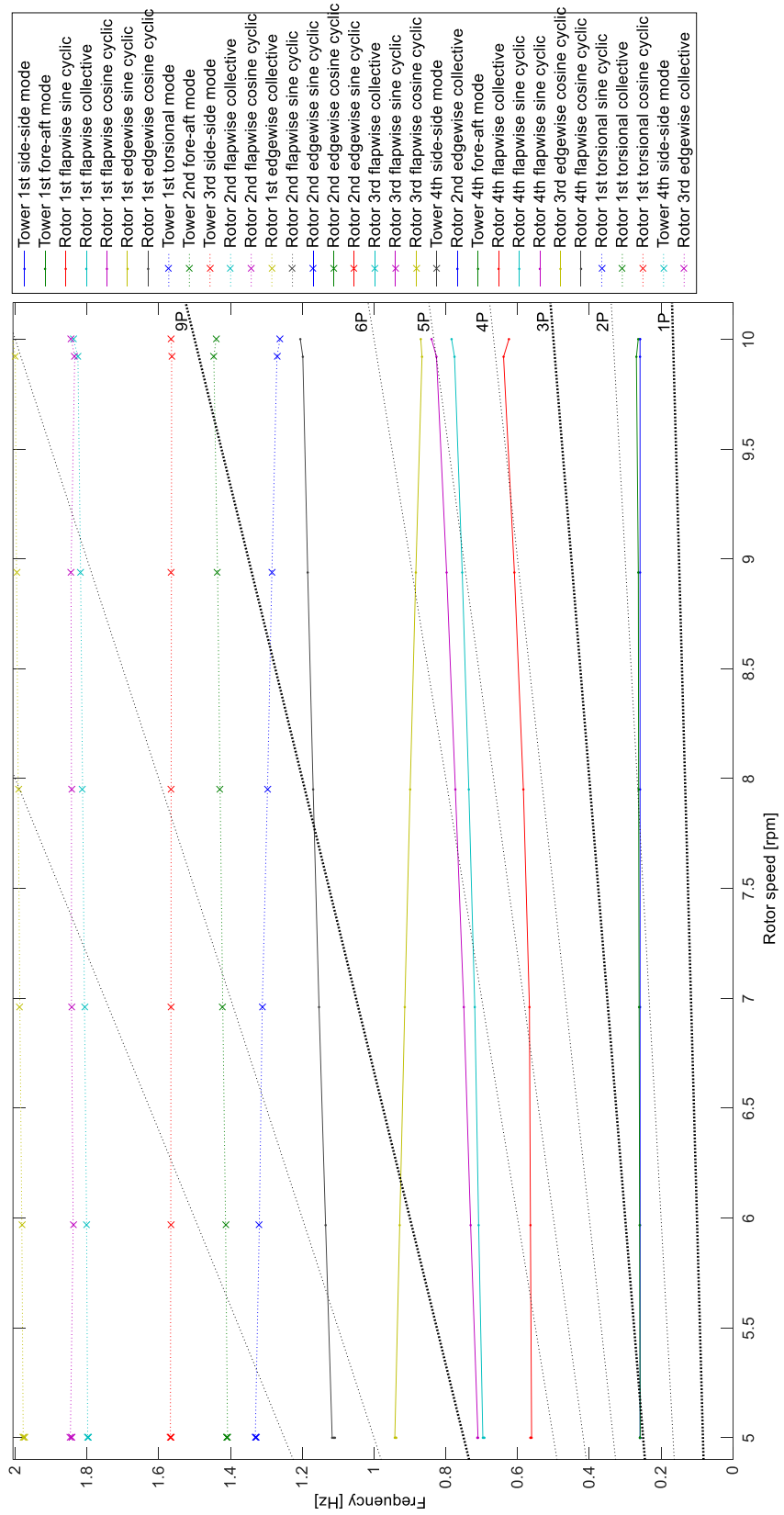

Figure 3-11: Campbell diagram

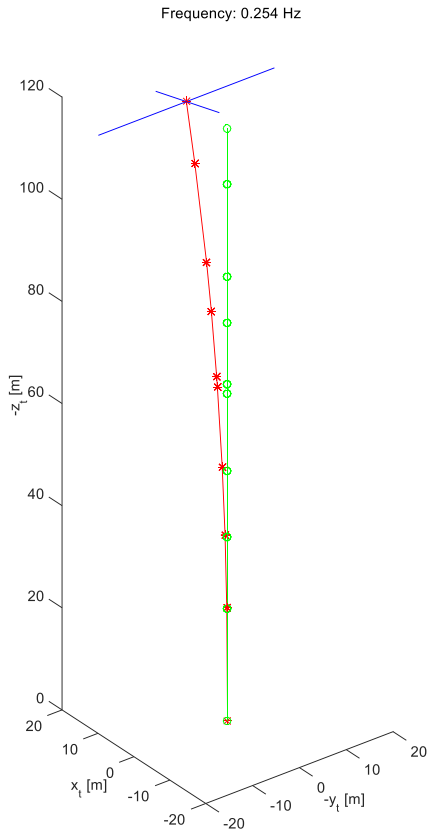

Figure 3-12: Tower first side-side mode shape

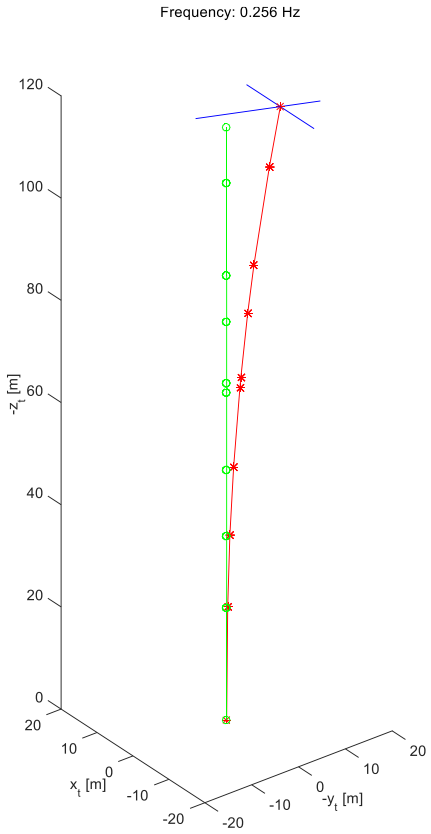

Figure 3-13: Tower first fore-aft mode shape

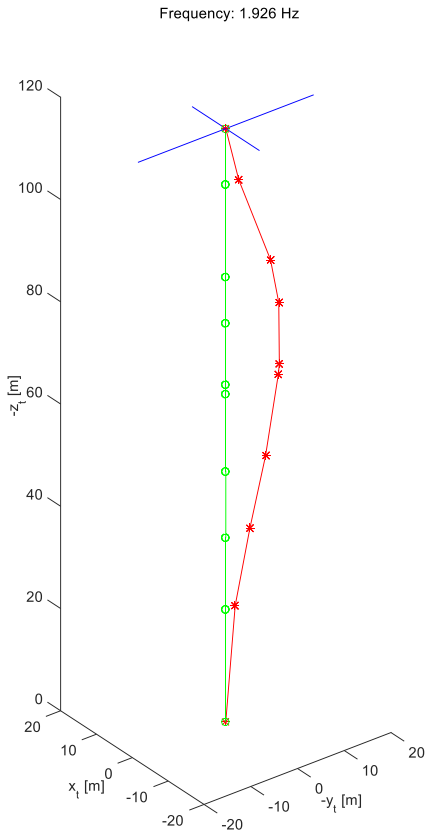

Figure 3-14: Tower second fore-aft mode

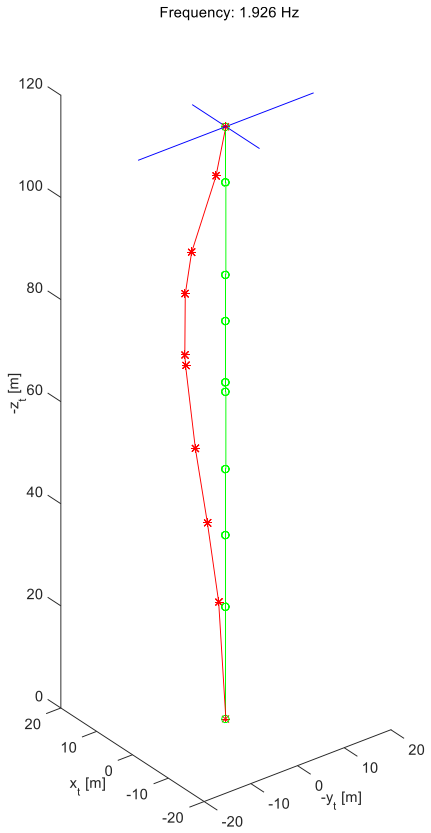

Figure 3-15: Tower second side-side mode

shape

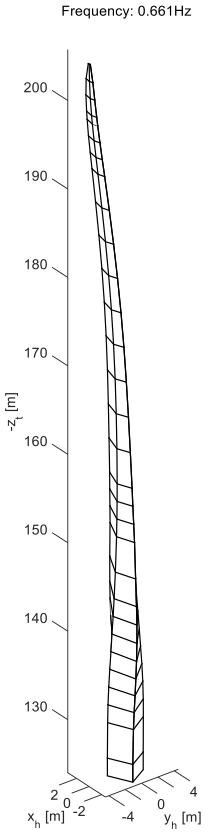

Figure 3-16: Blade first flapwise mode shape

shape

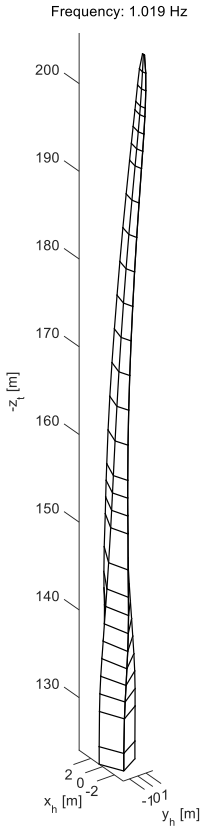

Figure 3-17: Blade first edgewise mode shape

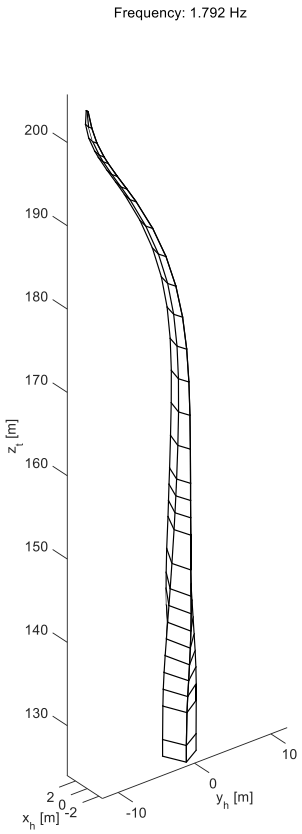

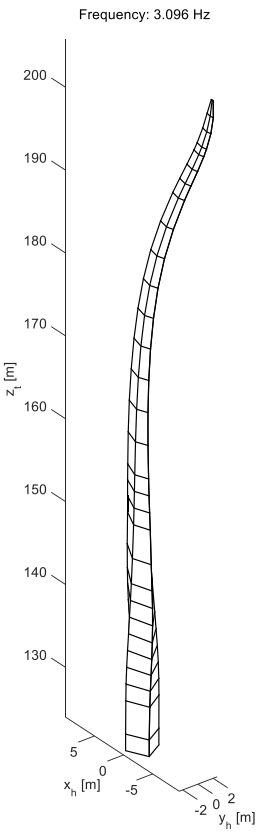

Figure 3-18. Blade second flapwise mode shape

Figure 3-19: Blade second edgewise mode shape

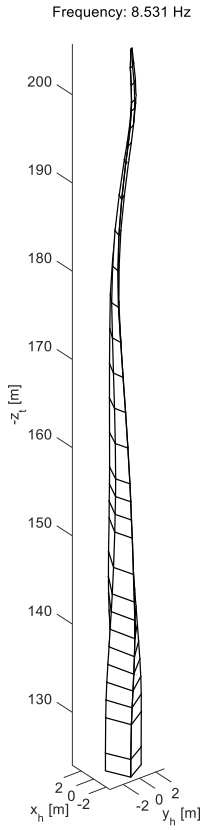

Figure 3-20: Blade first torsional mode shape

3.6 Pitch system

The pitch system consists of individual drives for each blade, which are mounted on the hub and connected to the pitch bearing. The connection of the blades via bearings have the benefit to pitch the blade in both directions clock and counter-clockwise without any structural limitation. Each pitch drive is controlled individually and requires a backup system in order to ensure a working pitch system in case of grid loss. Furthermore, the pitch drive is equipped with a passive brake system to keep the blade at any given position. The brake only releases when the system is energized. This ensures that the brake system is active during a grid loss with loss of accumulator power supply at the same time.

3.7 Rotor-Nacelle-Assembly

The complete Rotor-Nacelle-Assembly mass is 536.6 t. Together with the single mass of each component the mass moments of inertia are given in Table 3-9. The generator mass moment of inertia is defined with respect to the coordinates x_s, y_s, z_s, the nacelle

mass moment of inertia is defined with respect to the coordinates x_{tt}, y_{tt}, z_{tt} and the hub mass moment of inertia according to x_h, y_h, z_h (see Figure 2-1).
The center of gravity CG_{hub} and the appliance of the mass moment of inertia of the hub has the following coordinates in the shaft coordinate system: x_s = 0 m, y_s = 0 m, z_s = 6.2 m.
The center of gravity $CG_{generator}$ and the appliance of the mass moment of inertia of the generator has the following coordinates in the shaft coordinate system: x_s = 0 m, y_s = 0 m, z_s = 0m.
The center of gravity $CG_{nacelle}$ and the appliance of the mass moment of inertia of the nacelle has the following coordinates in the tower top coordinate system: x_{tt} = 0 m, y_{tt} = 1.5 m, z_{tt} = -3.05 m.
The yaw moment of inertia combined for all tower head components is 5.531E07 kgm².
Figure 3-21 shows the geometry and center of gravity positions.

Table 3-9: Mass and mass moment of inertia of nacelle hub and generator

	Mass	I_{xx}	I_{yy}	I_{zz}
Component	kg	kg m²	kg m²	kg m²
Nacelle	250000	7.05E06	2.48E06	7.19E06
Hub	104000	0.00E00	0.00E00	3.74E05
Generator	90000	0.00E00	0.00E00	5.22E05

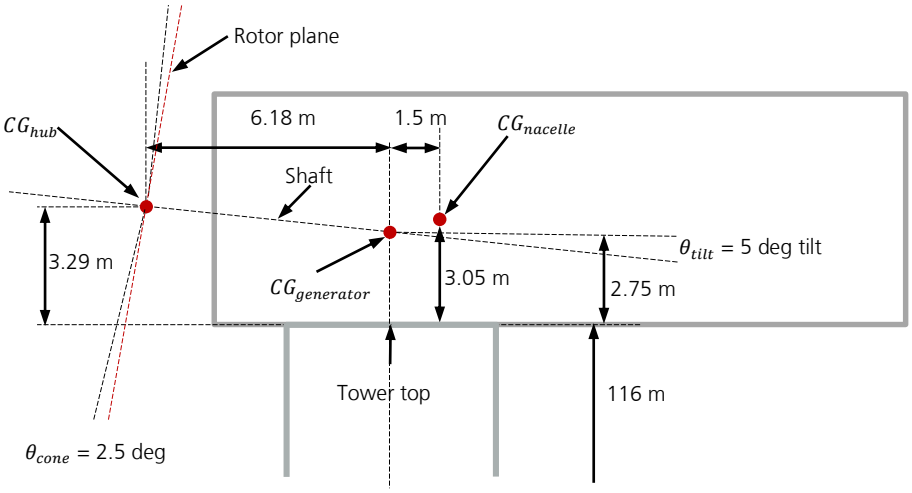

Figure 3-21: RNA geometry and center of gravity positions

4
Controller

This chapter contains a description of the control strategy, architecture, filters, control parameters tuning and the supervisory control strategy used in the IWES baseline controller. The controller is a further development of the controller used by DTU Wind Energy [9] and is inspired by Bossanyi's controller for the "NREL 5-MW Offshore Baseline Turbine" [10], in which the individual pitch controller is implemented as the most significant change.

4.1
Features of controller

The Fraunhofer IWES baseline controller for pitch-regulated, variable-speed wind turbines features both collective pitch control and individual pitch control capabilities including partial- and full-loading operation modes. The switch mechanisms smoothen the switching between partial- and full-load operations. The basic supervisory control functions including normal stop, emergency stop, over speed monitor and grid loss are implemented.
The controller uses the blade pitch angles and the electromagnetic generator torque to control the wind turbine. The aerodynamic gain scheduling is included to account for the effects of changing aerodynamics of the wind turbine for different wind speeds in the full-load operational region. The generator power error is also used as a feedback term in the collective pitch controller that keeps the pitch at its minimum below rated power. The individual pitch controller is used to reduce the loads above the rated wind speed. The current implemented features of the baseline Fraunhofer IWES controller are:

- Collective pitch PID controller, individual pitch PID controller and the generator torque PID controller based on classical control theory for both partial load operation and full load operation.
- Optimal generator torque-speed curve tracking combined with PID torque control in partial load operation.
- Aerodynamic gain scheduling for different wind speeds at full load region according to partial derivative of aerodynamic torque with respect to the collective pitch angle.
- Smooth switching between the partial load region and full load region.
- Drive train active damping.
- Basic supervisory control strategy including normal stop, emergency stop, over speed monitoring and grid loss.

4.2
Pitch and torque control

In this section, the strategy and algorithm of the baseline controller are presented. First, the two operational regions (partial load and full load) are described, and then the switching between these two regions is explained. Second, the aerodynamic gain scheduling and nonlinear gain are described. Third, the active drive train damping method is described. In the end, the individual pitch control algorithm used in the

baseline controller is presented. A block diagram of the entire controller is show in Figure 4-1.

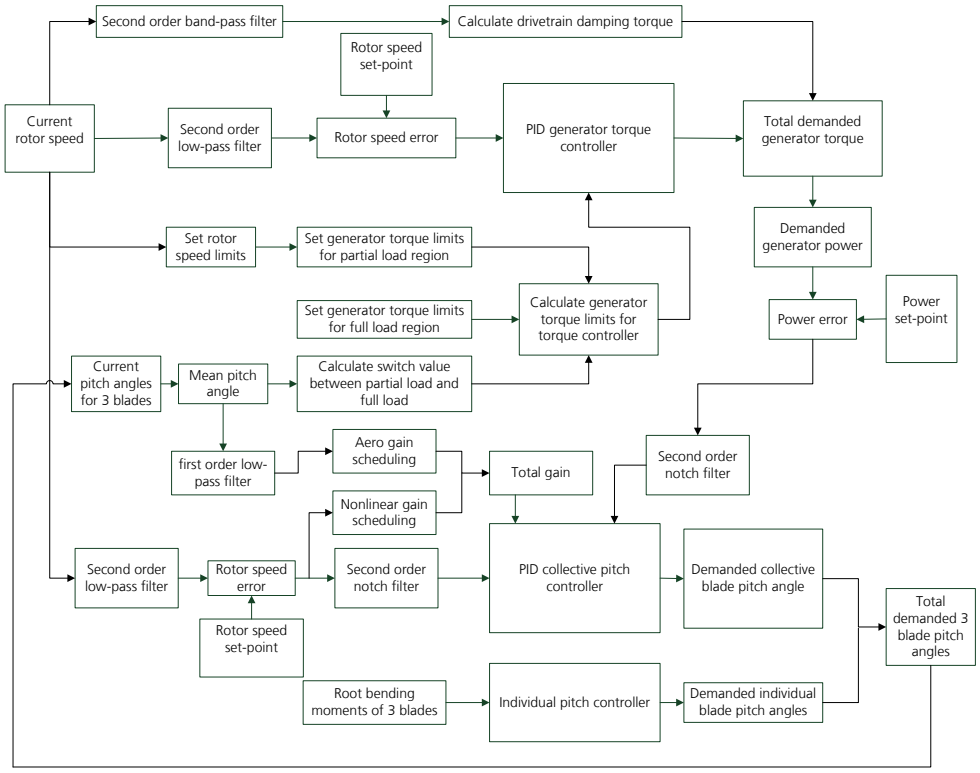

Figure 4-1: Block diagram of IWES baseline controller

4.2.1
Partial load operation

In the partial load region, the strategy is to track the tip-speed-ratio based on a balance between generator torque and aerodynamic torque to obtain a generator torque which keeps the operation point as close as possible at the optimal C_p. To avoid the feedback of higher frequency dynamics on the drive train, the rotor speed is filtered by a second order low-pass filter before it goes to the PID generator torque controller to compute the demanded generator torque $Q_{ref,k}$. This demanded generator torque is enforced by setting the torque limits for the PID torque controller to $Q_{min,k} = Q_{max,k} = K_{opt}\overline{\Omega}_k$ whenever the filtered rotor speed $\overline{\Omega}_k$ is not close to the minimum speed Ω_{min} or the rated rotor speed $\Omega_{r,k}$. When the filtered rotor speed is close to its bounds, these torque limits will be calculated using the interpolated factors $\sigma_{min,k}$ and $\sigma_{max,k}$ calculated by Eq. 4-1. The interpolation limits used for calculating $\sigma_{min,k}$ and $\sigma_{max,k}$ are $[\Omega_{min0}, \Omega_{min1}]$ and $[\Omega_{max0}, \Omega_{max1}]$. Then, the demanded generator torque will be computed by the PID generator torque controller based on the rotor speed error, where the rotor speed set point is either the minimum rotor speed or the rated rotor speed. The interpolation function used here is defined as follows [9]:

$$\sigma(x_0, x_1 : x) = \begin{cases} 0 & x < x_0 \\ a_3x^3 + a_2x^2 + a_1x + a_0 & x_0 < x < x_1. \\ 1 & x_1 < x \end{cases} \quad \text{Eq. 4-1}$$

The coefficients in Eq. 4-1 are described here.

$$a_3 = \frac{2}{(x_0 - x_1)^3},\ a_2 = \frac{-3(x_0 - x_1)}{(x_0 - x_1)^3}, a_1 = \frac{6x_0x_1}{(x_0 - x_1)^3}, a_2 = \frac{(x_0 - 3x_1)x_0^2}{(x_0 - x_1)^3} \quad \text{Eq. 4-2}$$

4.2.2 Full load operation

In the full load operation region, the generator torque set point is $P_{r,k}/\Omega_{r,k}$. The demanded collective pitch angle is obtained from a combined PID feedback of the rotor speed error and the power error. The rotor speed error is obtained as the difference between the second order low-pass filtered rotor speed and the rated speed. The power error is the difference between the demanded power and the rated power. Both errors are notch filtered around the frequency specified by the user for the value of the free-free drivetrain frequency. The power error feedback is important because it ensures that the demanded pitch angle is kept at the minimum pitch value until the rated power is reached.

The anti-windup is performed such that the controller will react quickly with increased pitch angle if the demanded power suddenly increases above the rated power. In each time step, the minimum pitch angle is added on the collective demanded pitch which is the summation of the proportional, integral and derivative terms expressed by Eq. 4-3.

$$\theta_{ref,k} = \max(\theta_{min,k}, (\theta_{P,k} + \theta_{I,k} + \theta_{D,k})) \quad \text{Eq. 4-3}$$

The value of the integral term to be used for the integration in the next time step is then recalculated as $\theta_{I,k} = \theta_{ref,k} - \theta_{P,k} - \theta_{D,k}$, which only makes a change to the integral term if the demanded pitch is equal to the minimum limit $\theta_{ref,k} = \theta_{min,k}$. Below rated power, where the proportional term is negative, in order to keep the rotor speed error close to zero by the PID controller, the integral term will be positive. If the demanded power is increased and gets closer to the rated power due to the reaction of the torque PID controller to an increased wind speed, then the proportional term will come close to zero, whereas the integral will still be positive and the resulting demanded pitch angle will be positive, whereby large power and speed variations are avoided.

4.2.3 Partial load and full load switching

The switching between partial load and full load is controlled by a first order low-pass filtered switching variable $S_{\theta,k}$ that is calculated by the interpolation function described in Eq. 4-1 using the filtered mean collective pitch angle. Two limits θ_{s1} and $\theta_{s2}$are used to specify the interpolation limits around the minimum pitch $\theta_{min,k}$ for the interpolation function defined in Eq. 4-1. As explained in section 4.2.2, the anti-windup algorithm of the PID pitch controller will ensure that the demanded pitch angle increases above its minimum value when the demanded power closes to the rated power. If the two angle limits are given to be equal, then a hard switching between partial load control and full load control is defined. Otherwise, this switching follows the function defined in Eq. 4-1 which results in a smooth switching while the response speed of the PID torque and pitch controller will be slower. The values of these two angle limits should be carefully selected.

4.2.4
Aerodynamic gain scheduling and nonlinear gain

The first order low-pass filtered mean of the blade pitch angle $\theta_{m,k}$ is used for the aerodynamic scheduling of the PID pitch controller. A quadratic function of the aerodynamic torque gain with collective pitch angle is assumed as follows:

$$\frac{\partial Q_A}{\partial \theta} = \frac{\partial Q_A}{\partial \theta}|_{\theta=0}\left(1 + \frac{\theta}{K_1} + \frac{\theta^2}{K_2}\right), \qquad \text{Eq. 4-4}$$

where Q_A is the aerodynamic torque, θ is the collective pitch angle and $\frac{\partial Q_A}{\partial \theta}|_{\theta=0}$ is the aerodynamic gain at zero pitch. The parameters in this expression, $K_1$and K_2, can be obtained from curve fitting to the derivative of the aerodynamic torque with respect to collective pitch angle assuming quasi-steady aerodynamics and frozen wake (constant induced velocities). In most of application, a linear fit is sufficient and it is assumed when $K_2 = 0$. In this case, K_1 is the angle at which the aerodynamic gain is doubled. Another approach is that $\left(1 + \frac{\theta}{K_1} + \frac{\theta^2}{K_2}\right)$ can be also obtained by a lookup table which is constructed from the derivative of the aerodynamic torque with respect to collective pitch angle by the user.

Besides to the aerodynamic gain scheduling, an additional feedback term is added to the PID pitch controller in order to improve the control quality in response to the gust. This feedback term depends on both rotor speed error contribution and the rate of change of the rotor speed error contribution, which are filtered by the second order low-pass filter to prevent the over reaction to the high frequency signal. Each contribution is scaled by a user-defined factor. Afterward, the sum of the two contributions is calculated. If the calculated value excess over 1.0, it is multiplied by a factor and added on the derivative term of the PID pitch controller. This non-linear feedback results in an additional pitch action when the rotor speed error is large, positive and fast increasing. The parameters used in this IWES baseline controller were selected to suppress over speed during gusts while maintain the control quality for normal turbulent wind.

4.2.5
Active drive train damping

As it is shown in Figure 4-1, the measured rotor speed is fed through a band-pass filter with the drivetrain torsional frequency as the center frequency. The filtered rotor speed, containing in-phase variations with the frequency around the drivetrain torsional frequency, is multiplied by a gain factor and added to the demanded generator torque calculated by the PID torque controller to give the total generator torque reference.

4.2.6
Individual pitch control

The individual pitch controller creates an additional zero-mean pitch demand for each blade which is added to the collective demanded pitch angle. The individual pitch angles are calculated from the measured blade root bending moments to minimize the asymmetrical out-of-plane loads on the rotor produced by inhomogeneity of turbulence, wind shear, yaw misalignment, tower shadow and aerodynamic asymmetry of the rotor. The basic idea is to transform the measured 3 blade root bending moments from the rotating reference frame into two orthogonal components (yaw moment and tilt moment) in the non-rotating reference frame. The same method is used in the helicopter control and electrical motor control, where it is known as the

Coleman transformation [11] or Park transformation. The transformed two load components are thought of as representing the asymmetrical load components in tilt and yaw directions. Two PID controllers are applied on the two orthogonal components in order to calculate the additional two pitch angles. Afterward, an inverse Coleman transformation calculates the appropriate individual pitch demands for the three blades in the rotating reference frame, which can be then added to the collective pitch demand calculated before. The individual pitch control is used to minimize the asymmetrical out-of-plane loads.

The Coleman transformation can be written as follows:

$$\begin{bmatrix} L_d \\ L_q \end{bmatrix} = \frac{2}{3}\begin{bmatrix} \cos(\varphi) & \cos(\varphi + 2\pi/3) & \cos(\varphi + 4\pi/3) \\ \sin(\varphi) & \sin(\varphi + 2\pi/3) & \sin(\varphi + 4\pi/3) \end{bmatrix}\begin{bmatrix} L_1 \\ L_2 \\ L_3 \end{bmatrix}, \qquad \text{Eq. 4-5}$$

where φ is the rotor azimuth angle, $L_i (i = 1,2,3)$ are the three blade loads in the rotating reference frame, L_d and L_q are the transformed two load components which are orthogonal to each other in the non-rotating reference frame. The corresponding inverse Coleman transformation is described in Eq. 4-6.

$$\begin{bmatrix} L_1 \\ L_2 \\ L_3 \end{bmatrix} = \begin{bmatrix} \cos(\varphi) & \sin(\varphi) \\ \cos(\varphi + 2\pi/3) & \sin(\varphi + 2\pi/3) \\ \cos(\varphi + 4\pi/3) & \sin(\varphi + 4\pi/3) \end{bmatrix}\begin{bmatrix} L_d \\ L_q \end{bmatrix} \qquad \text{Eq. 4-6}$$

An offset angle can be added to the azimuth angle in the inverse Coleman transformation to compensate for any time lag caused by the controller time step. Two PID controllers are designed to regulate the transformed two load components to their set-points. In the current implementation the two PID controllers are the same as each other, although they can be different to account for the differences due to yaw dynamics or the tower dynamics. Non-zero set-point can be used if required to create a yawing moment or a nodding moment for other controller purpose, but for this application zero set-points are used.

A second order low-pass filter with the corner frequency at 1P frequency is used in series with each of the two PI controllers. The inverse Coleman transformation generates 1P pitch signals at the three blades which compensate for the 1P loading, which is caused by rotational sampling of turbulence wind field together with wind shear, yaw misalignment and imbalance, which dominates the fatigue loads of the blades and the main shaft. In the non-rotating reference frame, for example, the loads at yaw bearing, nacelle and the tower, the individual pitch controller compensates the low frequency variations in tilting and yawing moments while it does not have much effect on the 3P loads. However it is possible to reduce this 3P loads by means of an additional second individual pitch controller, which operates in parallel with the current individual pitch controller. In this case the Coleman transformation is applied with the second harmonic azimuth angles. This will reduce the 2P loads on the rotational components which results in the loads reduction on 3P loads on the non-rotating components. In the current status, the second harmonic individual pitch controller is not implemented yet.

The two PI controllers for generating the individual pitch demanded angles are subject to limits on their outputs, which means after the inverse Coleman transformation the maximum amplitude of the individual pitch actions are limited. This limit can be specified by the user for each of the two PID controllers. These limits are reduced to zero in order to fade out the individual pitch actions if the power output is below rated power.

4.3 Filters

In this section the filters used in this controller are described and the parameters for the first order low-pass filter, the second order low-pass filter and the second order band pass filter are tuned.

4.3.1 First order low-pass filter

In this controller the first order low-pass filter is mainly used to filter out the high frequencies in the measured blade pitch angle and the interpolated switch values for switching between partial load and full load. The continuous-time transfer function of the first order low-pass filter is expressed as follows:

$$G(s) = \frac{\tau}{s+\tau}, \qquad \text{Eq. 4-7}$$

where, τ is the time constant. For filtering the measured blade collective pitch angle, τ is set to be equal to 1P rotational period. Figure 4-2 shows the bode plot of this filter.

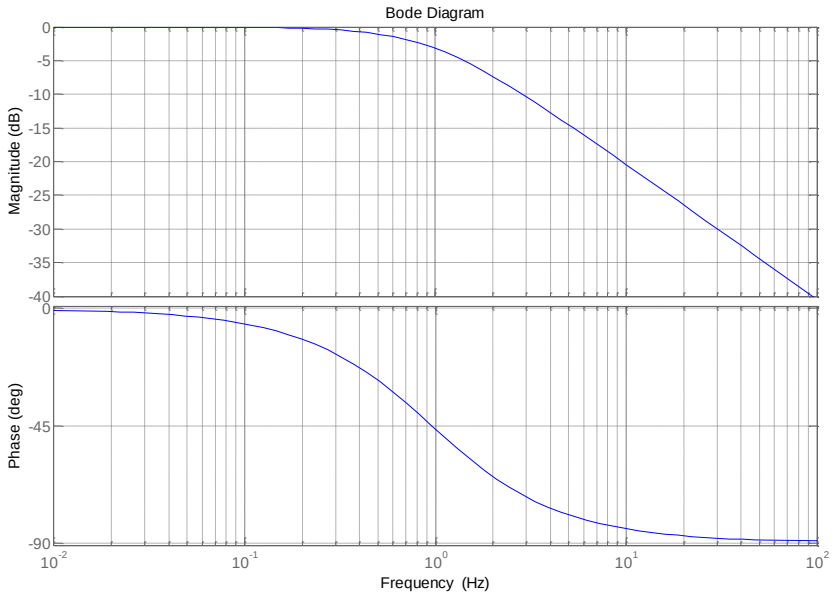

Figure 4-2: Bode diagram of the first order low-pass filter

4.3.2 Second order low-pass filter

The second order low-pass filter is mainly used to filter out the high frequencies in the measured generator speed which will be fed into to the PID pitch controller. The continuous form of the second order low-pass filter is expressed as follows:

$$G(s) = \frac{\omega_0^2}{s^2+2\zeta_0\omega_0 s+\omega_0^2}. \qquad \text{Eq. 4-8}$$

The cut-off frequency $\omega_0 = 5.1496$ rad/s and the damping ratio $\zeta_0 = 0.7$ are tuned and selected for the second order low-pass filter. Figure 4-3 shows the Bode plot of this second order low-pass filter expressed by Eq. 4-8 using the parameters listed above.

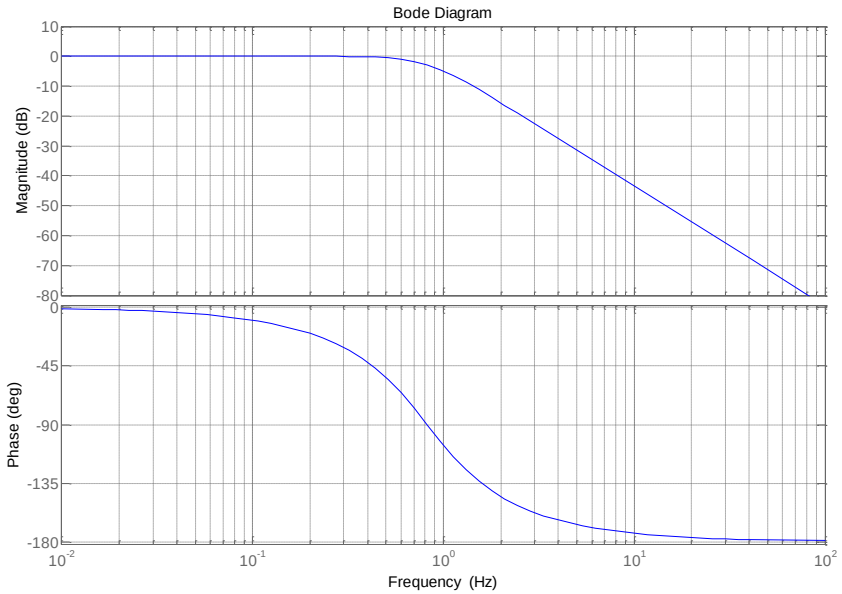

Figure 4-3: Bode diagram of the second order low-pass filter

4.3.3
Second order band-pass filter

In this implementation, a second order band-pass filter, shown in Figure 4-4, is designed to filter the rotor speed signal which will be multiplied by a gain factor to get the generator torque for the drivetrain damping. The continuous-time representation of the filter can be expressed as the following transfer function.

$$G(s) = \frac{s(1+\tau s)}{s^2+2\zeta_0\omega_0 s+\omega_0^2} \qquad \text{Eq. 4-9}$$

Here, ω_0 corresponds to the frequency of the first resonant free-free drive train torsional mode, ζ_0 is the damper ratio and is chosen fairly large to obtain the robust performance and τ is the time constant to compensate the phase lag. In this implementation it is hardcoded as zero. The following parameter values are selected for this band-pass filter:

$$\omega_0 = 9.6133 \text{ rad/s}, \ \zeta_0 = 0.7, \tau = 0.$$

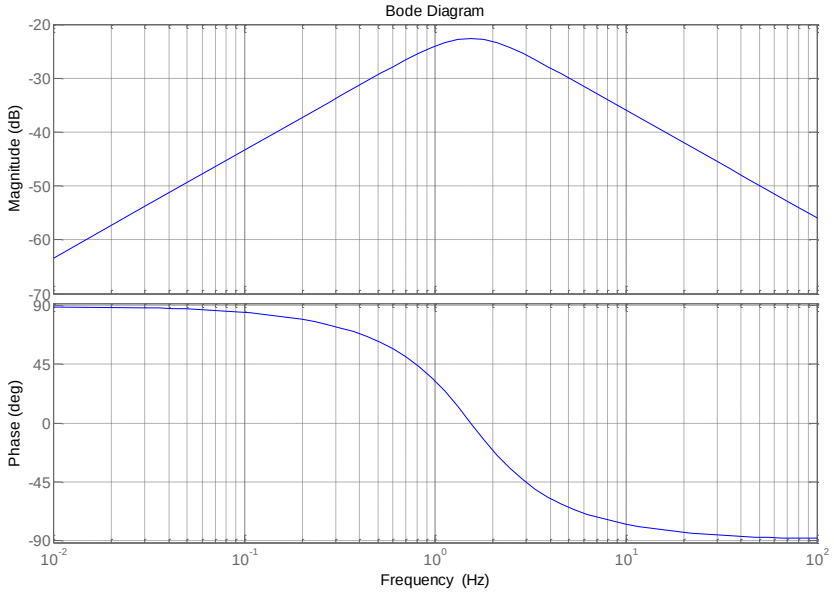

Figure 4-4: Bode diagram of the second order band-pass filter

4.4 Supervisory control

The supervisory control algorithm includes the procedure for normal turbine shutdown, over-speed monitor and the logic for determining failures of grid loss. Moreover, a suitable fade out of individual pitch contribution is considered during the wind turbine shutdown procedures.

4.4.1 Shut-down procedures

The shut-down of the wind turbine during the simulation can be triggered by the user input or by the over speed monitor depending on the load cases simulated. The pitch rate for different shutdown procedures is defined by the user. In Table 4-1 the different shutdown procedures that have been implemented are shown.

Table 4-1: Shut-down procedures

Shutdown procedure	Collective pitch controller action	Generator torque controller action
Normal Shutdown	Feather the blades with the collective slower pitch rate given by the user (e.g. 4 deg/s) to the maximum pitch angle	The generator torque is reduced to zero linearly within the time period defined by the user
Emergency Shutdown	Feather the blades with the collective faster pitch rate defined by user (e.g. 6 deg/s) to the maximum pitch angle position	The generator torque is reduced to zero
Grid Loss Shutdown	Feather the blades with the collective slower pitch rate defined by user (e.g. 4 deg/s) to the maximum pitch angle	The generator torque is reduced to zero

5
Control parameter tuning

This section presents some simulation results to explain the control parameter tuning process and the performance of the IWES baseline controller. The parameter tuning used in the current controller is also presented. The effect of the load reduction is demonstrated by comparing the result with and without individual pitch control.

5.1
Parameter tuning for generator torque and collective pitch controller

5.1.1
Step response simulation

To tune and evaluate the performance of the IWES baseline controller, a step response simulation with the deterministic wind speed is firstly performed. Typical quantities, e.g. wind speed, pitch angle, rotor speed and generator power, are plotted over time to show the results. The wind speed starts from 3 m/s and is stepped up to 25 m/s with a 1 m/s step every 50 s. The simulation is performed using the tuned parameters of the PID generator torque and PID collective pitch controller listed in Table 5-1 and Table 5-2.

Table 5-1: Parameters tuned for PID torque controller

	Value	Unit
Optimal generator constant	5.21743E+06	Nm s^2/rad^2
Proportional gain	3.12634E+07	Nm s/rad
Integral gain	7.01549E+06	Nm/rad
Differential gain	0	Nm s^2/rad

Table 5-2: Parameters tuned for PID collective pitch controller

	Value	Unit
Proportional gain	0.9848	rad s/rad
Integral gain	0.1582	rad/rad
Differential gain	0.0	rad s^2/rad
Proportional power error gain	4.0E-07	rad/W
Integral power error gain	4.0E-07	rad s/W
Linear aero gain scheduling	11.1189	deg

The results of wind speed step response of the IWT-7.5-164 turbine are presented in Figure 5-1. In the partial load region when the wind speed is less than 11 m/s, the controller regulates the generator torque and speed for optimal tip speed ratio λ_D (8.4) tracking while trying to keep the pitch angle constant to the optimal value (zero degree for the IWT-7.5-164). In this way, it extracts the maximum power out of the wind. It can be seen from the yellow curve of the blade pitch angle that the peak shaver takes action at the wind step from 10 m/s to 11 m/s (t = 450 s). In the full load region the

wind speed is higher than 11 m/s, the PID collective pitch controller regulates the rotor speed to the rated value that is 10 rpm and the PID generator torque controller keeps the constant rated generator power. The result shows that the step response of the pitch angle and rotor speed does not present big overshoots and oscillations. The response of the rotor speed is almost identical over the whole range between 11 m/s and 25 m/s, this indicates that the gain scheduling in the PID collective pitch controller works properly. The PID generator torque controller keeps the generator power to 7.5 MW with a small deviation. In the full load region (starting from t = 500 s) a sinusoidal oscillation (3P frequency) of the blade pitch can be obtained which is caused by the individual pitch control. The out-of-plane deflection of the blade has its maximum at the rated wind speed. This goes hand in hand with the thrust force of the rotor which has (in case of pitch controlled variable speed turbines) its maximum at the rated wind speed. It can be seen that PID generator torque controller, PID collective pitch controller and PID individual pitch controller show good performance for step-up response.

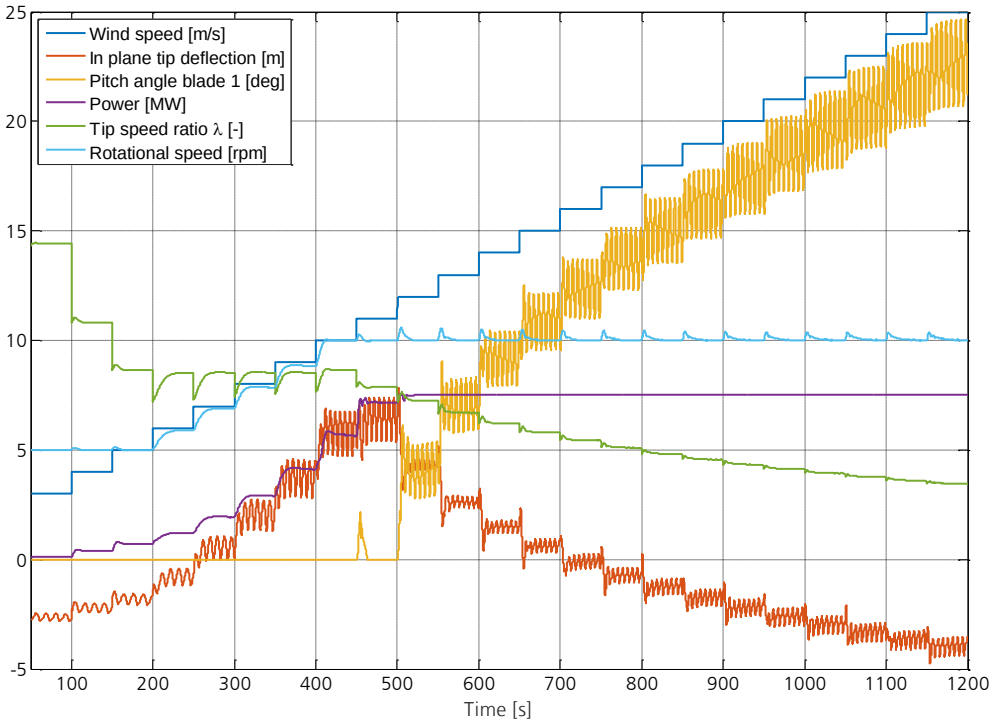

Figure 5-1: Step response between cut-in and cut-out

5.1.2 Power production simulation

Secondly, a power production simulation with normal turbulence model (NTM) at 13 m/s is performed using the control parameters listed in Table 5-1. Figure 5-2, Figure 5-3, Figure 5-4 and Figure 5-5 show that the controller achieves smooth transitions between the partial load and the full load operation. The rotor speed is regulated at 10 rpm with small variation less than 3% in the full load region. At around 220 s, 350 s, 450 s and 500 s, the wind speed becomes less than the rated wind speed on average, the rotor speed is reduced accordingly and the collective pitch angle is also reduced

towards zero, which demonstrates the controller behaves properly during the transient simulation around rated wind speed.

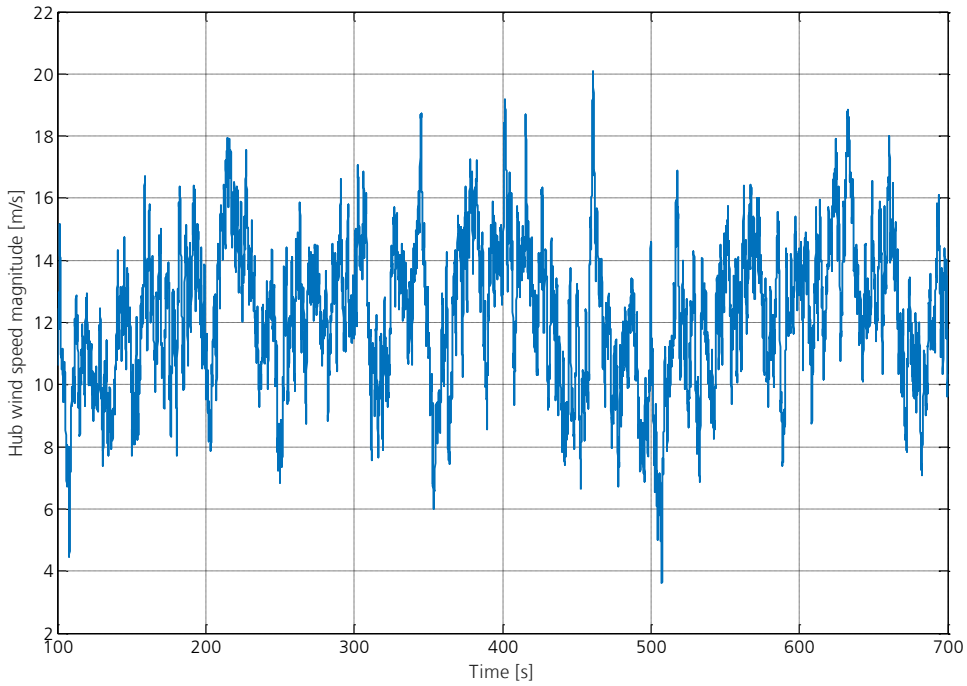

Figure 5-2: Transient simulation result (wind speed) around rated wind speed at 13 m/s with NTM

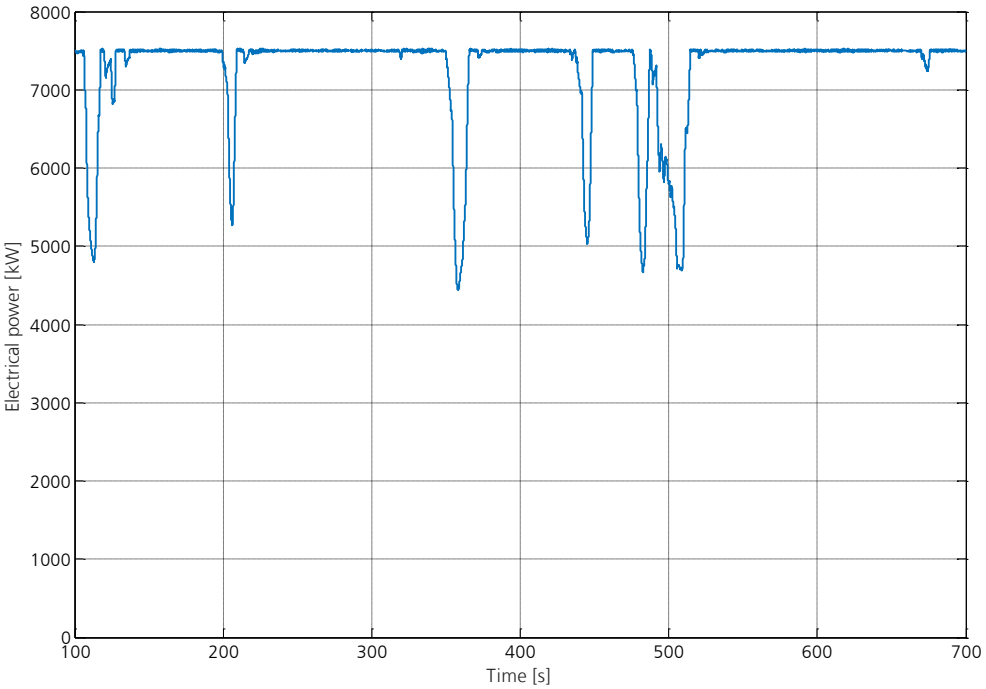

Figure 5-3: Transient simulation result (electrical power) around rated wind speed at 13 m/s with NTM

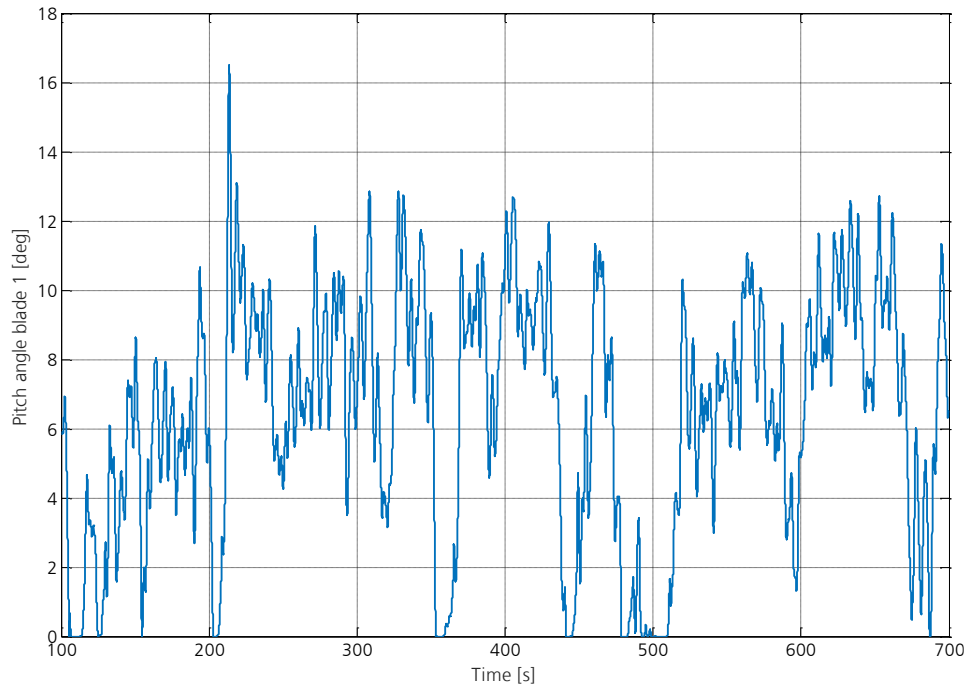

Figure 5-4: Transient simulation result (pitch angle) around rated wind speed at 13 m/s with NTM

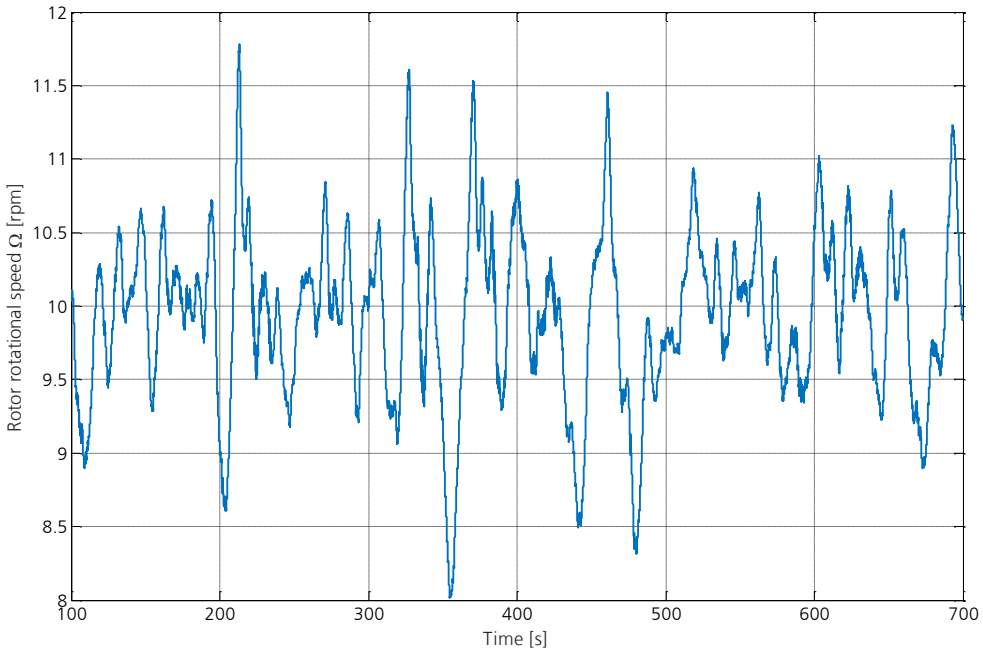

Figure 5-5: Transient simulation result (rotor speed) around rated wind speed at 13 m/s with NTM

5.2 Parameter tuning for individual pitch controller

The PID individual pitch controller is tuned by examining the effect of individual pitch control on the blade root out-of-plane bending moments. The simulation is performed using the following tuned parameters of the PID individual pitch controller listed in Table 5-3. The other control parameters are kept the same as used in Section 5.1.

Table 5-3: Parameters tuned for the PID individual pitch controller

	Value	Unit
Proportional gain	0.14	rad s / rad
Integral gain	0.08	rad / rad
Differential gain	0	rad s^2 / rad
1st order low-pass filter corner frequency	0.22	Hz
1st order low-pass filter damping ratio	0.7	

A power production simulation with a constant wind field at 13 m/s is used to evaluate the performance of the PID individual pitch controller. Figure 5-6 shows a part of the simulation results from 140 s to 300 s in order to show the pitch activities of the 3 blades during the power production caused by the individual pitch controller.

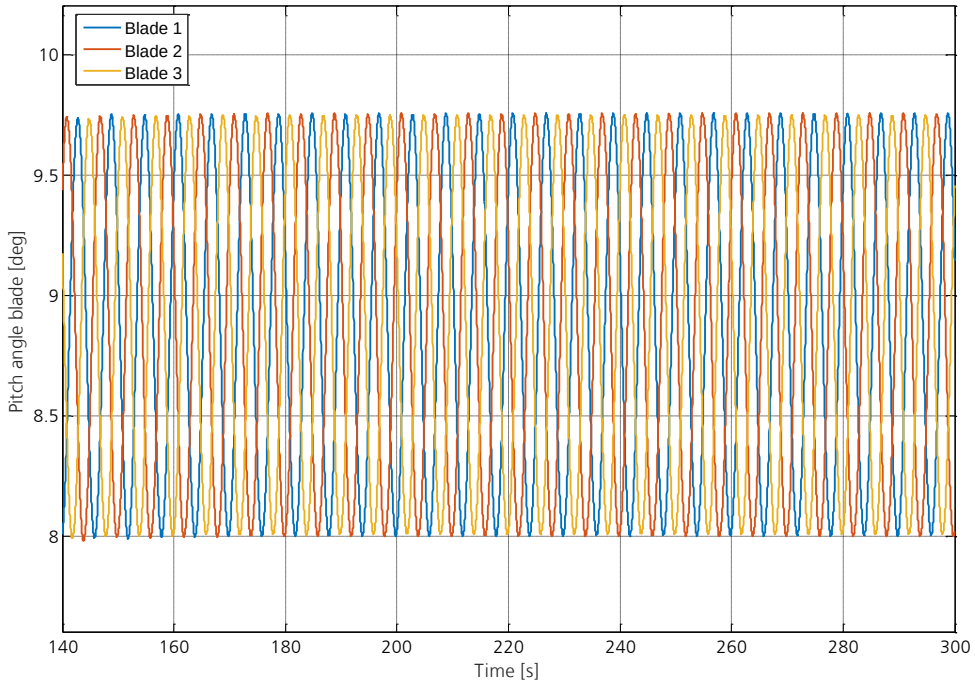

Figure 5-6: Individual pitch angles of the 3 blades

The time series of out-of-plane root bending moment M_x at blade 1 is plotted in Figure 5-7, which demonstrate clearly the loads reduction on the out-of-plane bending moment at the root of the blade by switching on the individual pitch control.

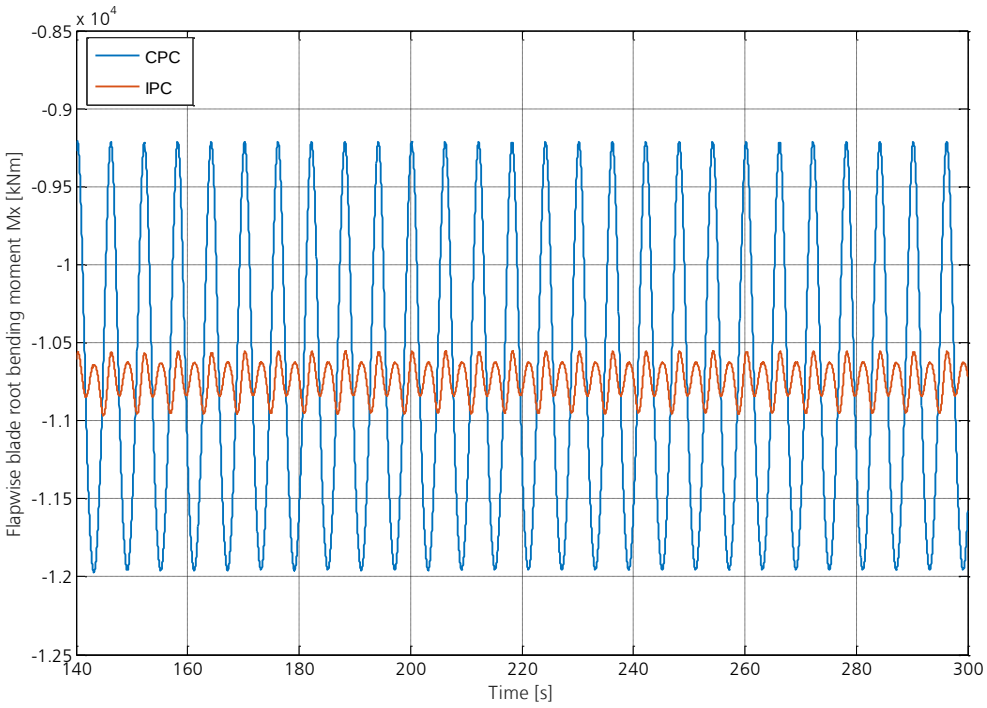

Figure 5-7: Blade 1 out-of-plane root bending moment comparison with and without individual pitch control

Appendix A.
Aerodynamic characteristics of the original airfoils

In this appendix are presented, by means of plots and diagrams, the aerodynamic characteristics and the geometrical description for the original airfoils. Different approaches are employed to determine the aerodynamic characteristics of the original airfoils: for the root circle the data were based on literature sources; for the IWES-A1 600-180 the data were computed with RFOIL [12] in forced transition on the leading edge. The remaining airfoil coefficients were estimated via XFOIL [13] in forced transition on the leading edge.

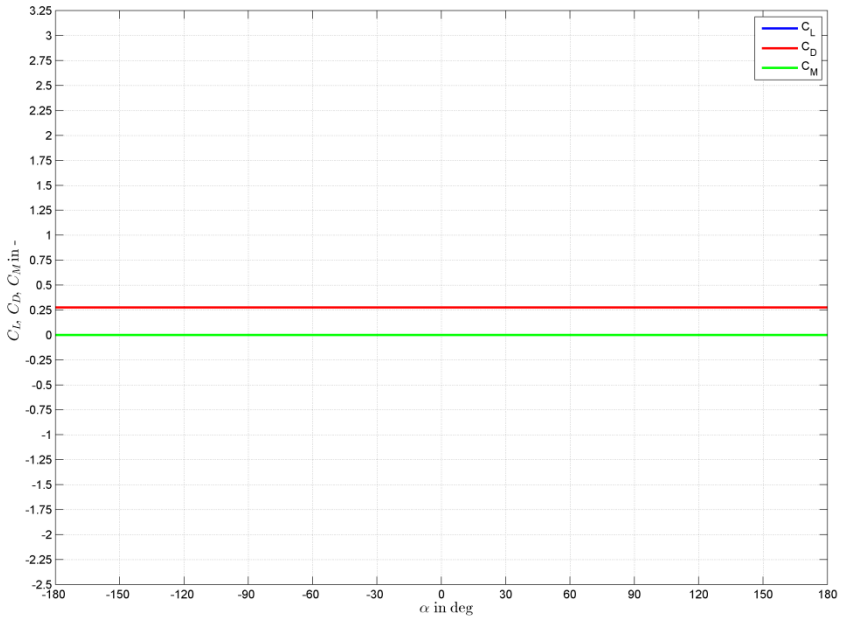

Figure A-1: Circle polars

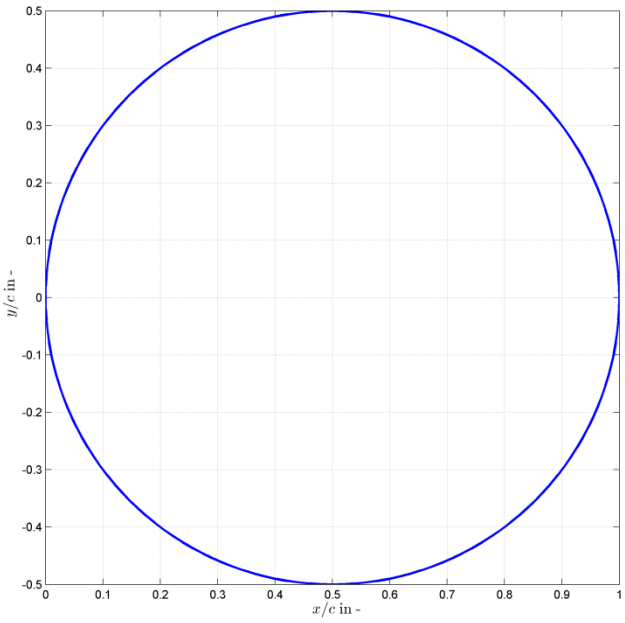

Figure A-2: Circle geometry

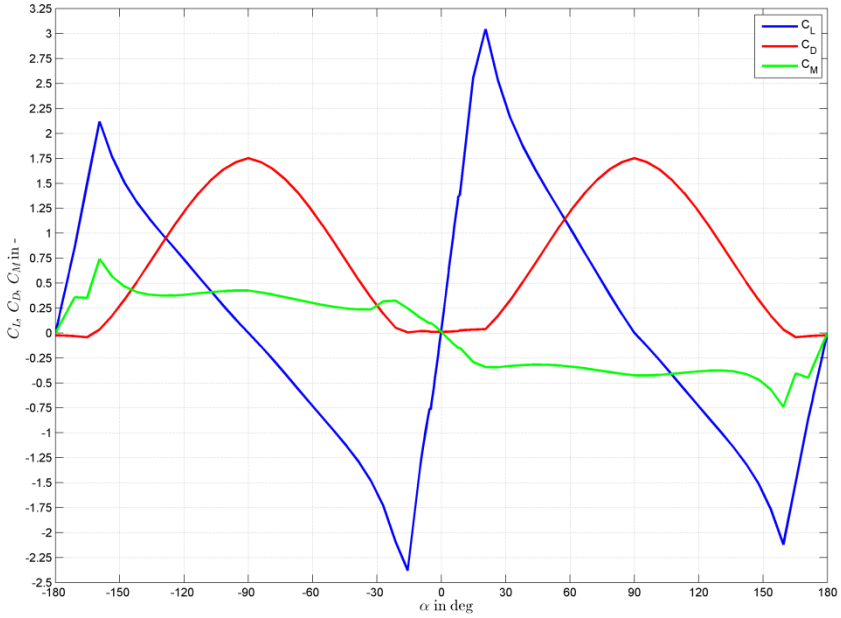

Figure A-3: IWES-A1600-180 polars

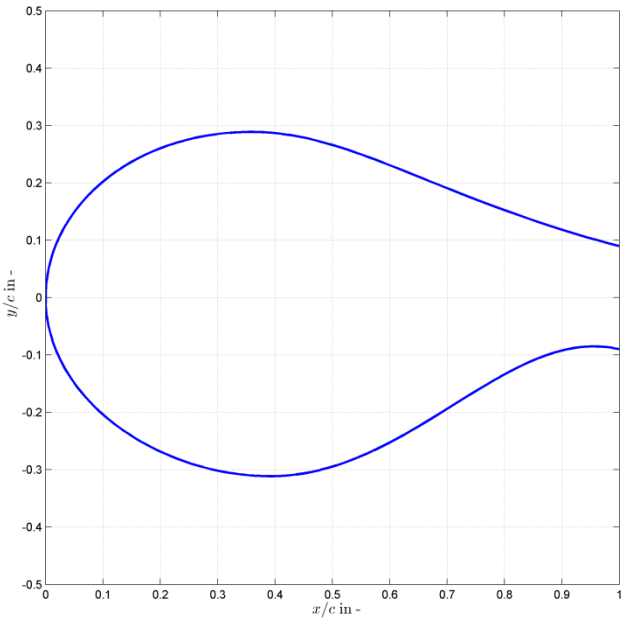

Figure A-4: IWES-A1600-180 geometry

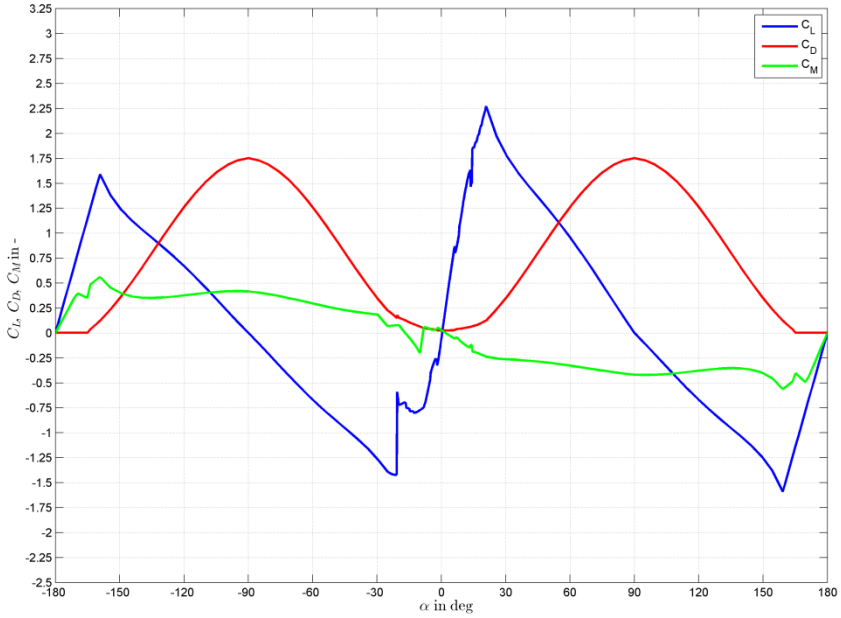

Figure A-5: IWES-A1 500-100 polars

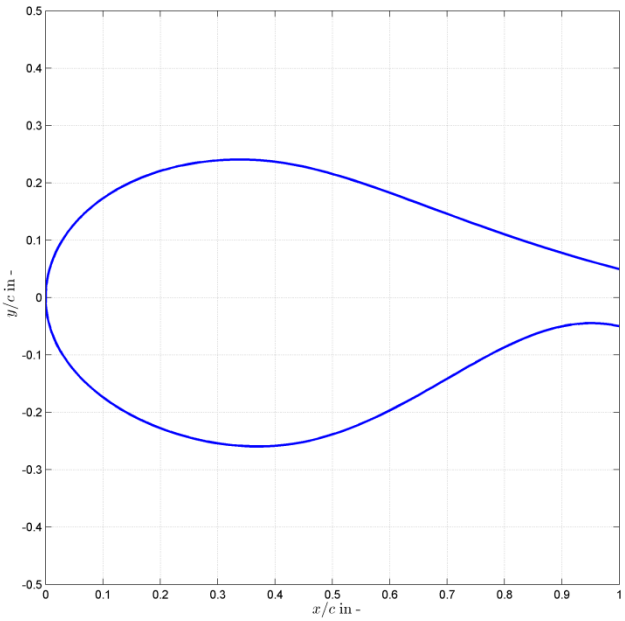

Figure A-6: IWES-A1 500-100 geometry

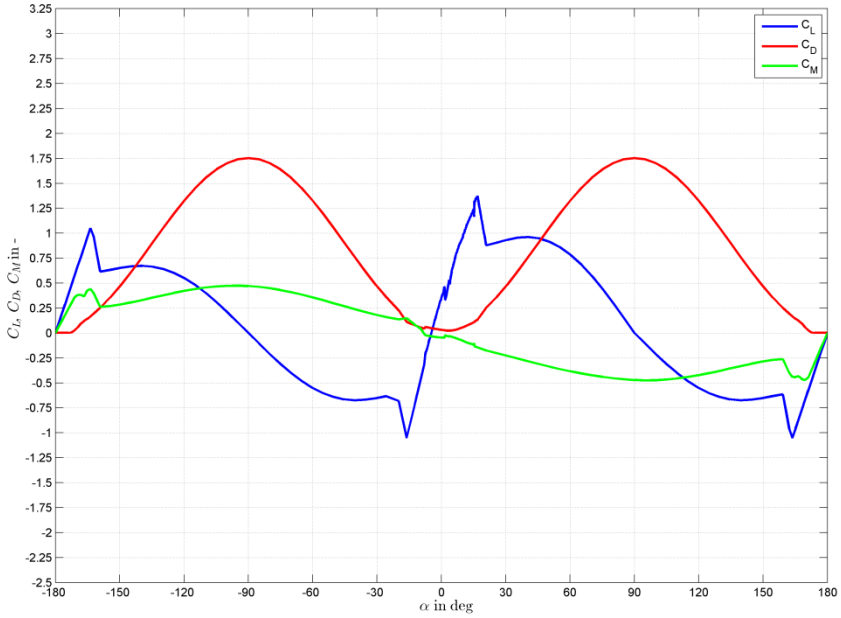

Figure A-7: IWES-A1 400-050 polars

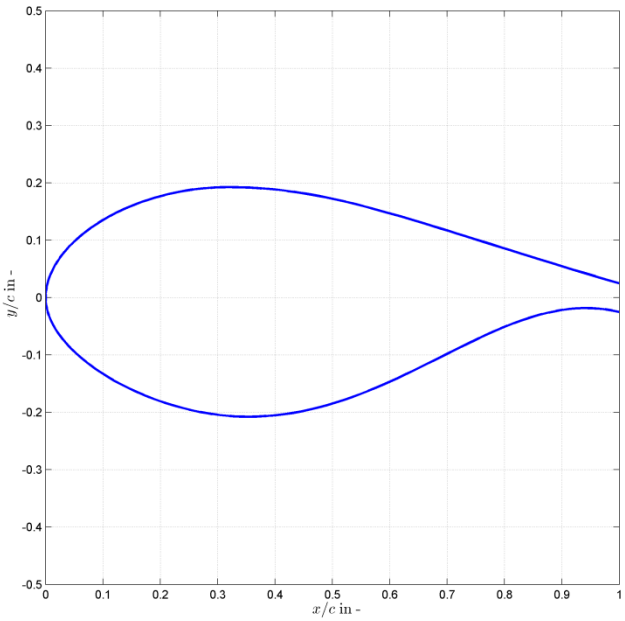

Figure A-8: IWES-A1 400-050 geometry

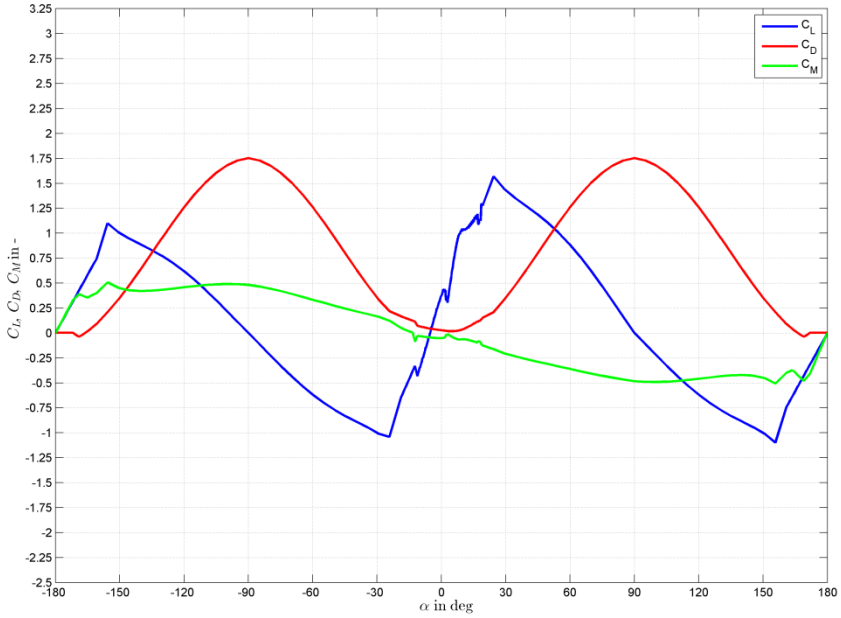

Figure A-9: DU 00-W2-350 polars

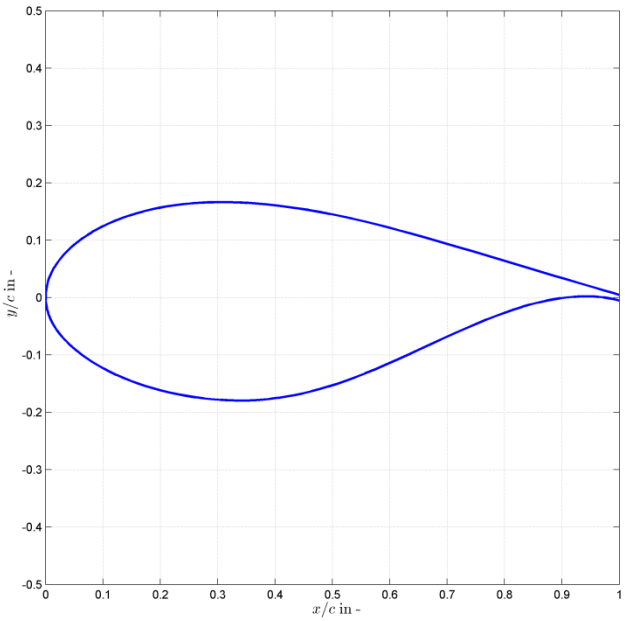

Figure A-10: DU 00-W2-350 geometry

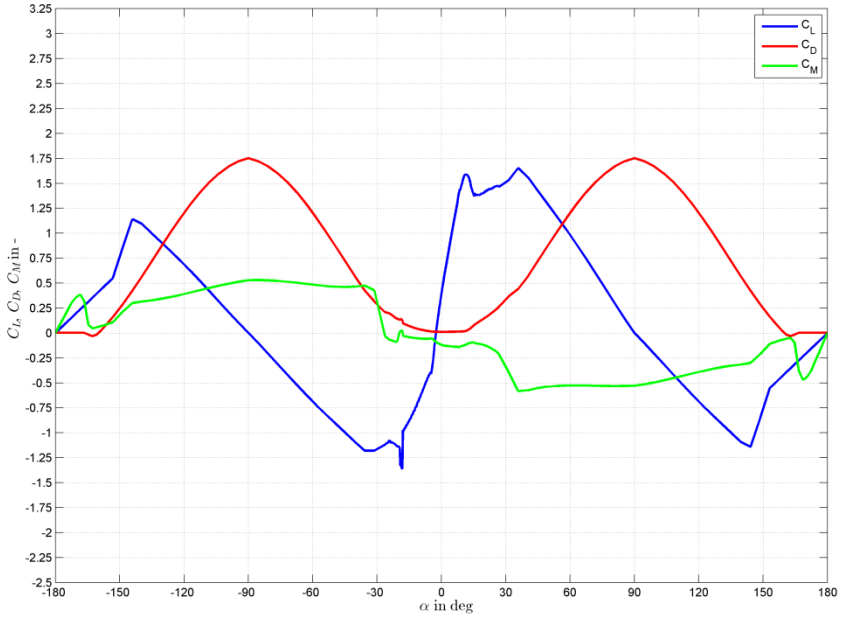

Figure A-11: DU 91-W2-250 polars

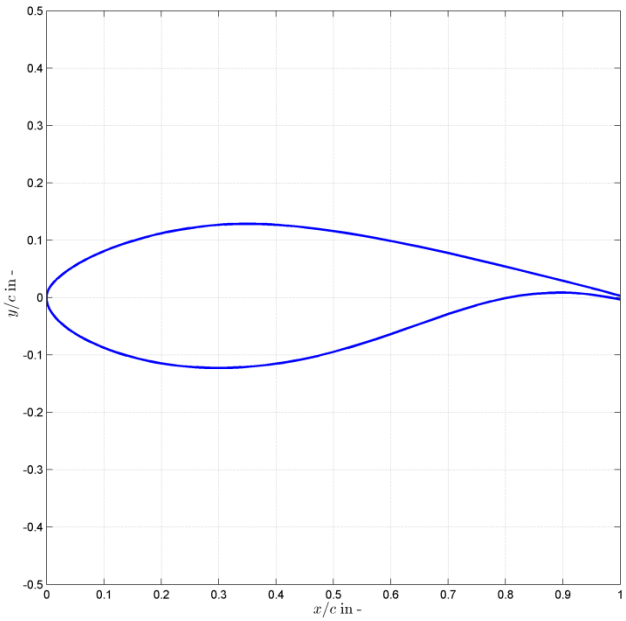

Figure A-12: DU 91-W2-250 geometry

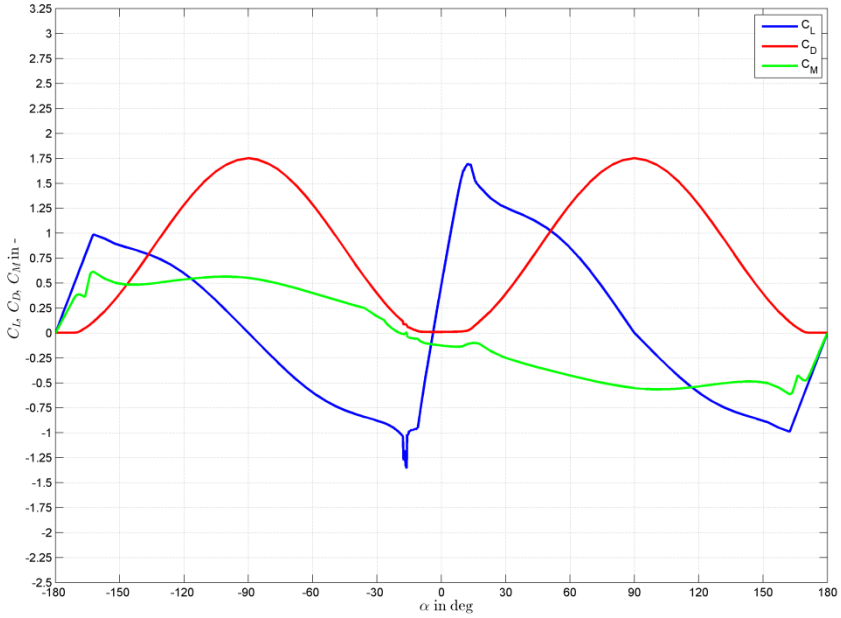

Figure A-13: DU 08-W-210 polars

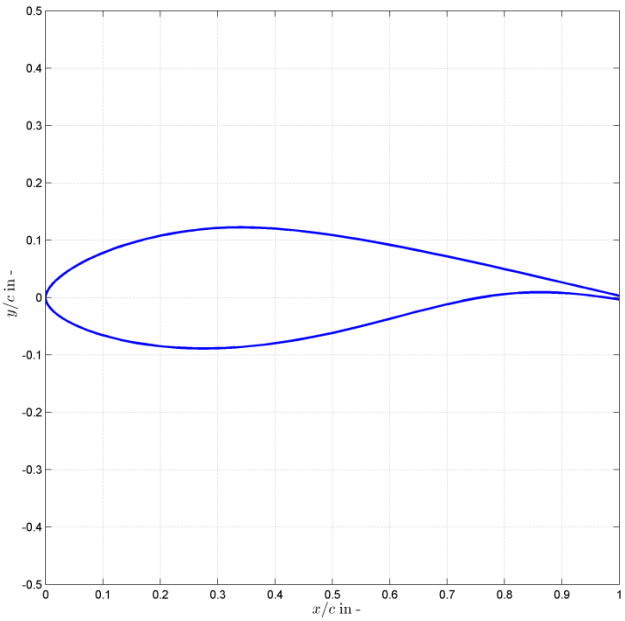

Figure A-14: DU 08-W-210 geometry

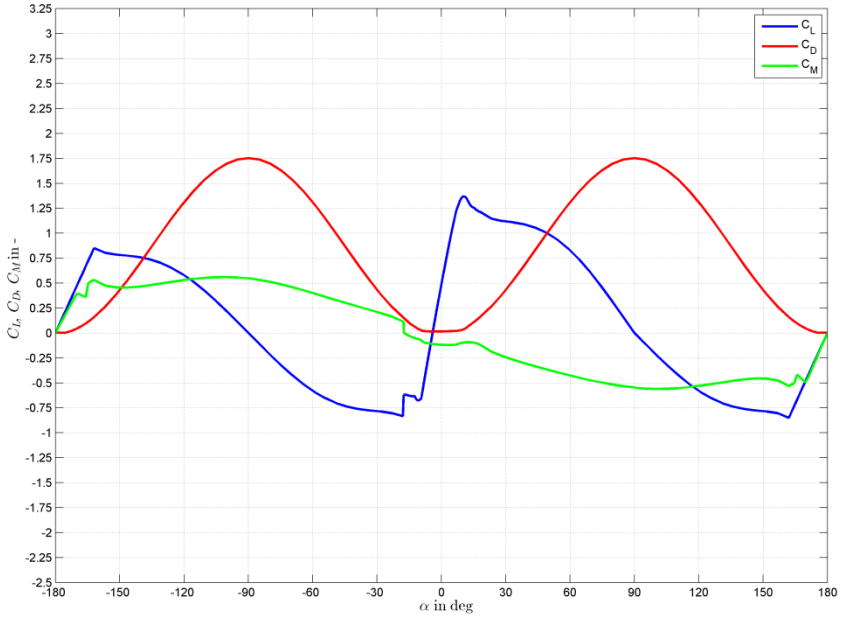

Figure A-15: DU 08-W-180-6.5 polars

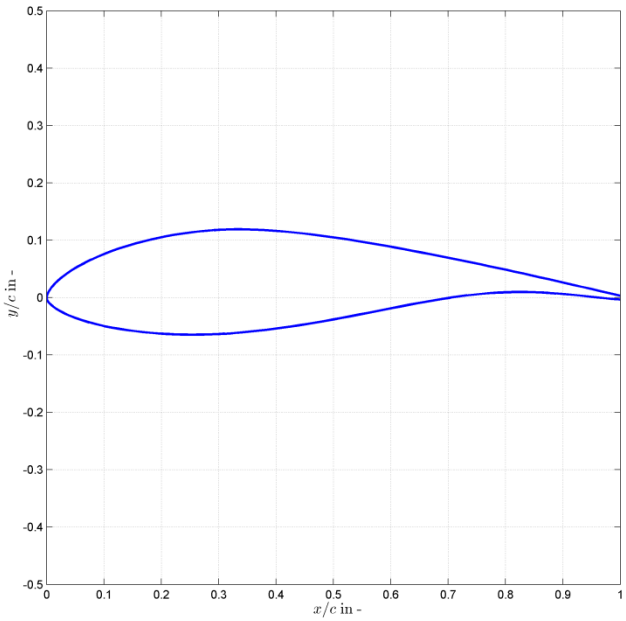

Figure A-16: DU 08-W-180-6.5 geometry

Appendix B.
Aerodynamic characteristics of the blended airfoils

In this Appendix are presented, by means of plots and diagrams, the aerodynamic characteristics and the geometrical description for the blended airfoils. Different approaches are employed to determine the aerodynamic characteristics of the blended airfoils: for the station 1-2 the data were based on literature sources; for the stations 3-6 the data were computed with RFOIL [12] in forced transition on the leading edge. The remaining airfoil coefficients were estimated via XFOIL [13] in forced transition on the leading edge. The aerodynamic coefficients of the sections were determined for the Reynolds numbers given in Table B-1.

Table B-1: Reynolds numbers used for the determination of the airfoil coefficients

Station	Re [-]	Station	Re [-]
1	1.50E+06	17	7.50E+06
2	1.70E+06	18	7.60E+06
3	2.10E+06	19	7.70E+06
4	2.70E+06	20	7.80E+06
5	3.50E+06	21	7.80E+06
6	4.40E+06	22	7.80E+06
7	5.20E+06	23	7.70E+06
8	5.90E+06	24	7.60E+06
9	6.30E+06	25	7.40E+06
10	6.50E+06	26	7.20E+06
11	6.80E+06	27	6.80E+06
12	7.00E+06	28	6.60E+06
13	7.10E+06	29	5.80E+05
14	7.10E+06	30	4.40E+06
15	7.20E+06	31	4.80E+05
16	7.30E+06		

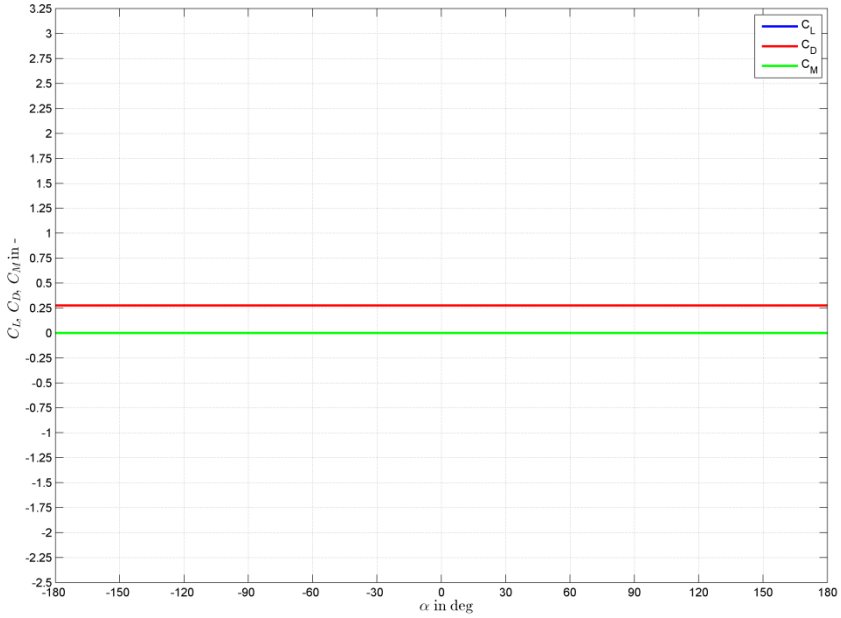

Figure B-1: Section 1 polars

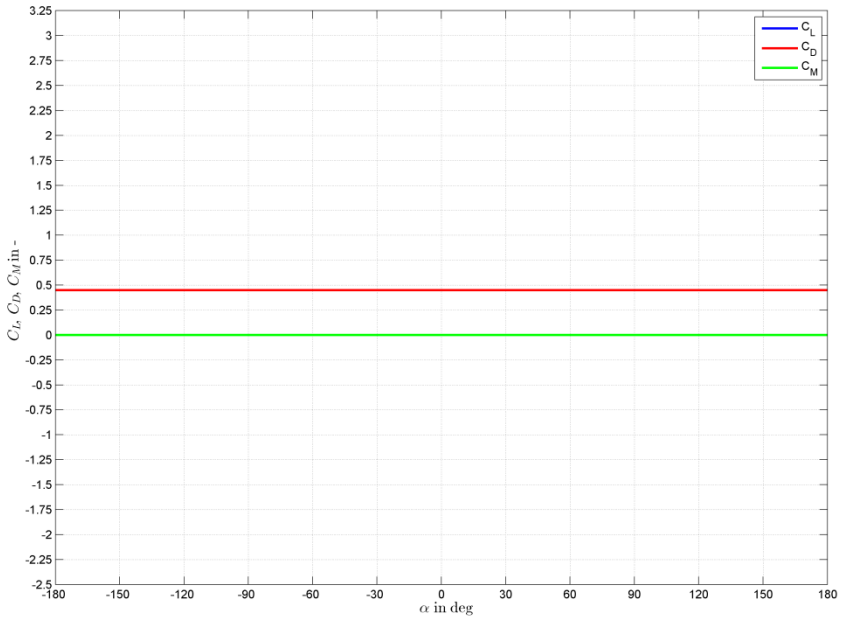

Figure B-2: Section 2 polars

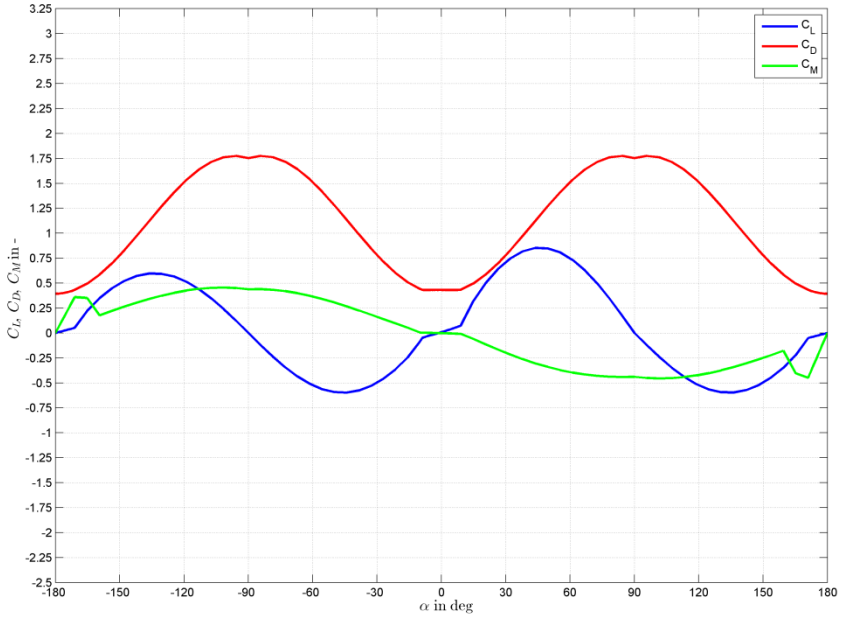

Figure B-3: Section 3 polars

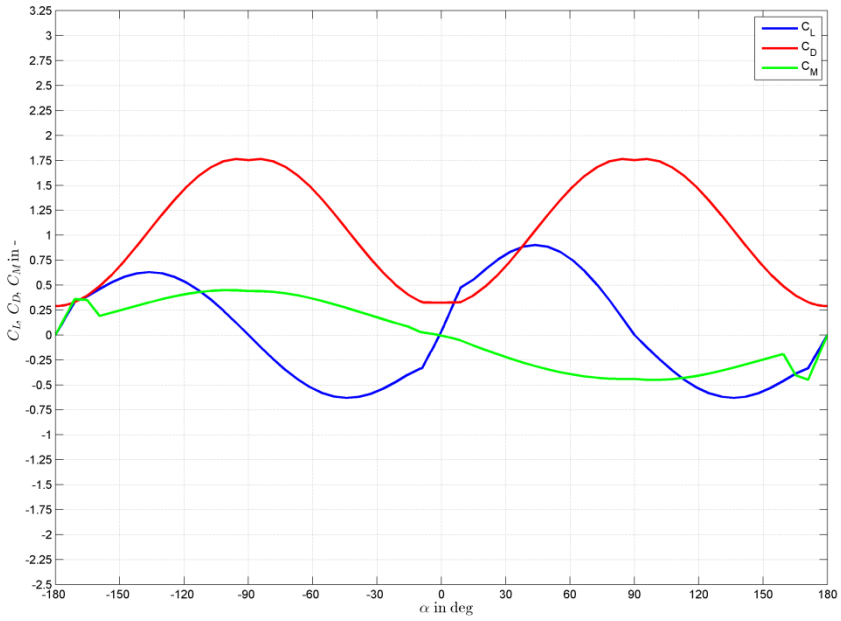

Figure B-4: Section 4 polars

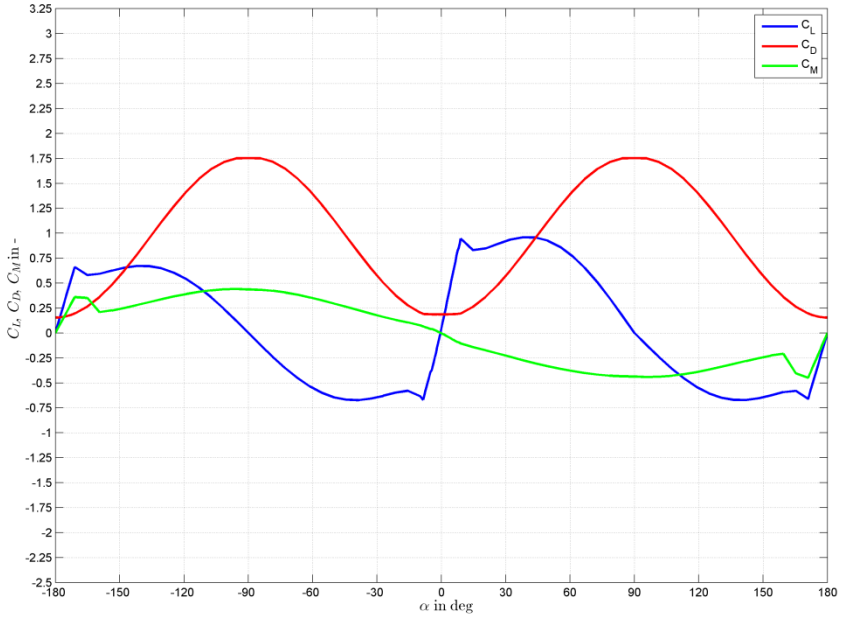

Figure B-5: Section 5 polars

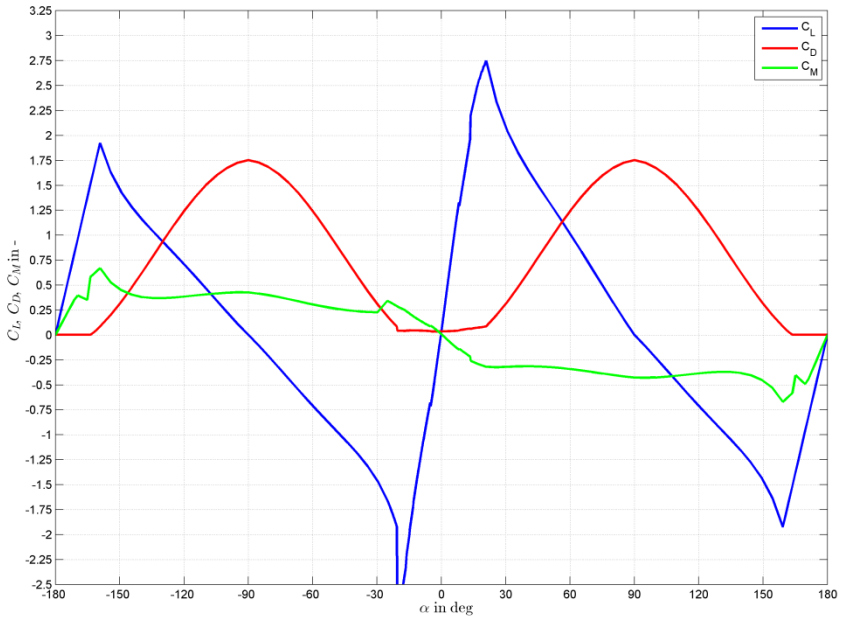

Figure B-6: Section 6 polars

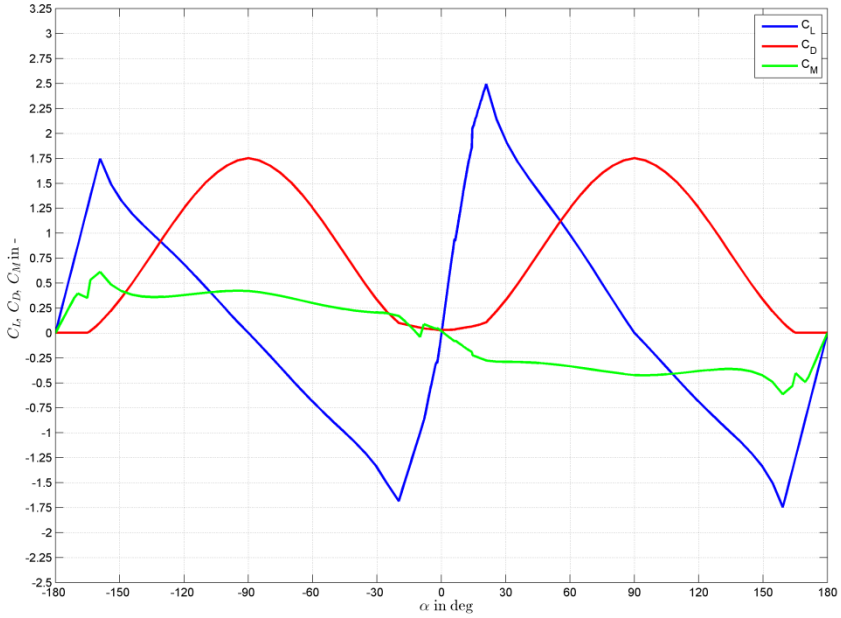

Figure B-7: Section 7 polars

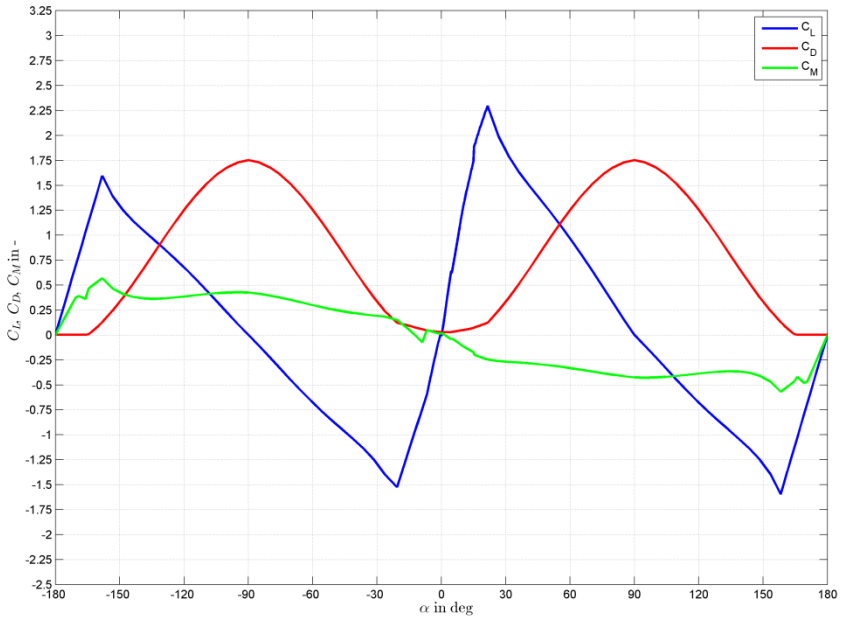

Figure B-8: Section 8 polars

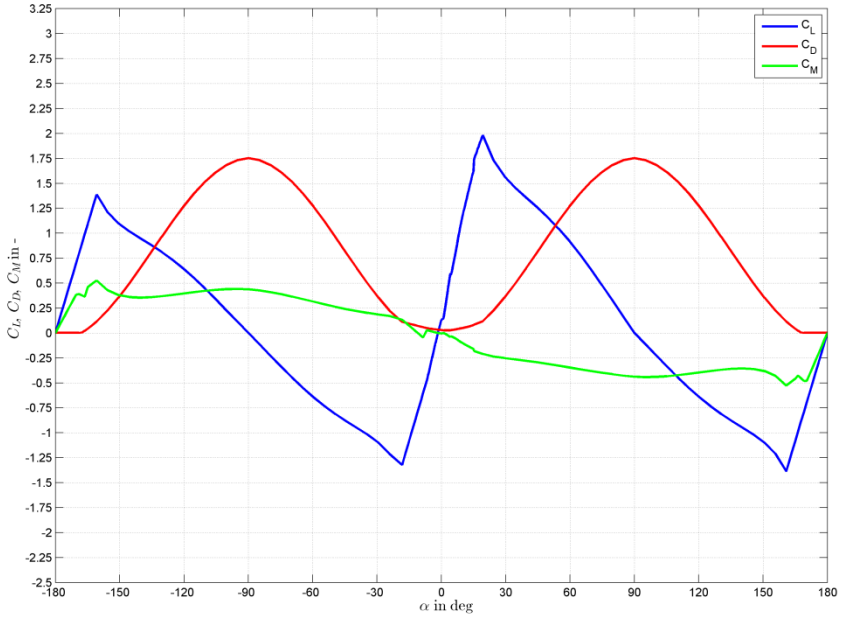

Figure B-9: Section 9 polars

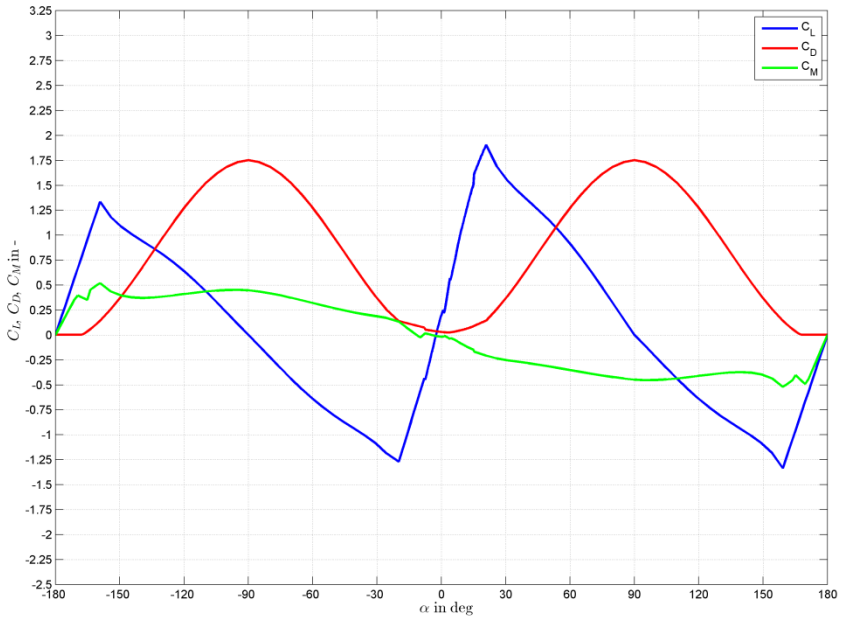

Figure B-10: Section 10 polars

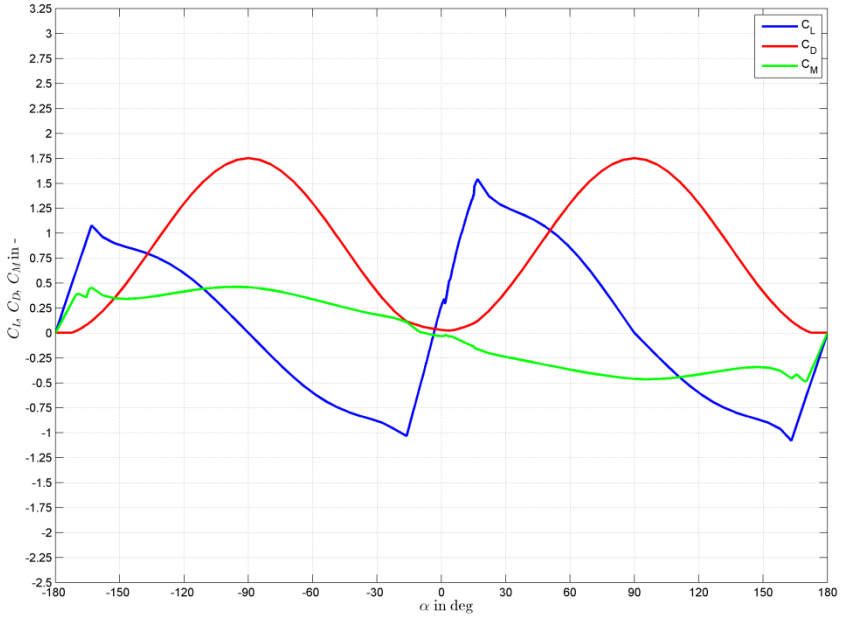

Figure B-11: Section 11 polars

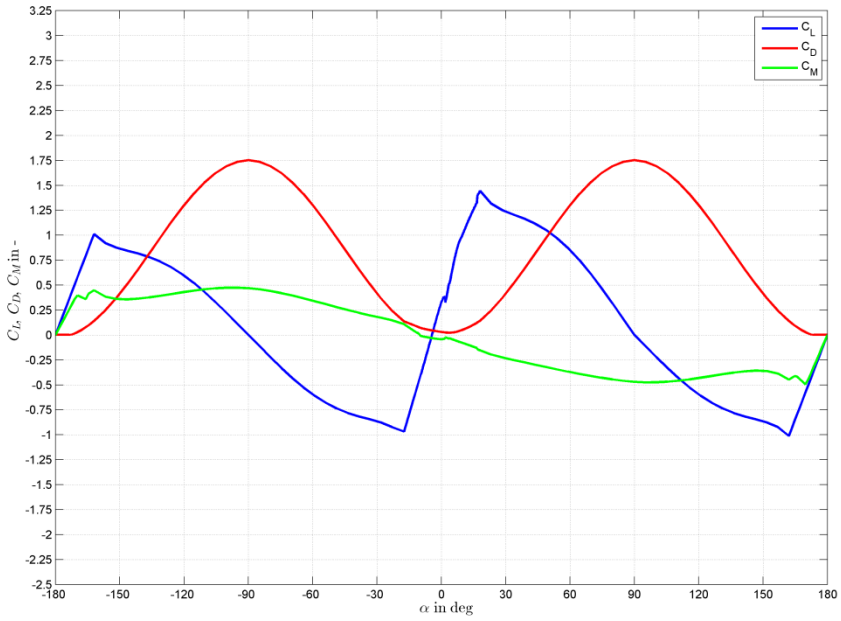

Figure B-12: Section 12 polars

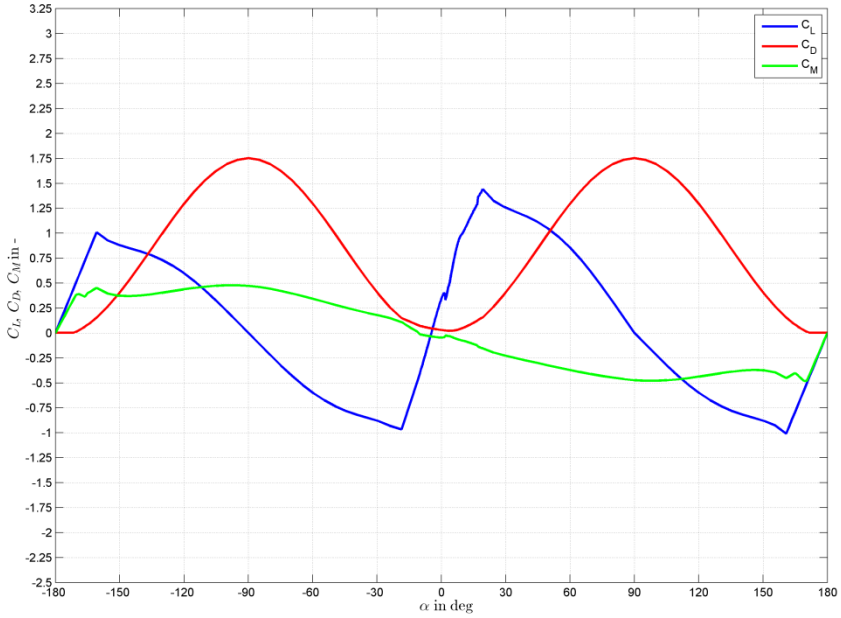

Figure B-13: Section 13 polars

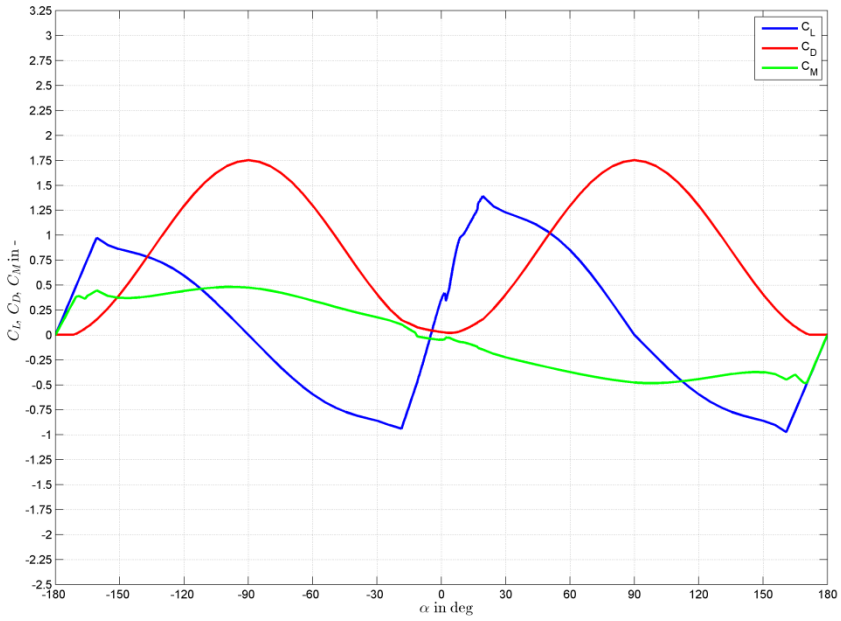

Figure B-14: Section 14 polars

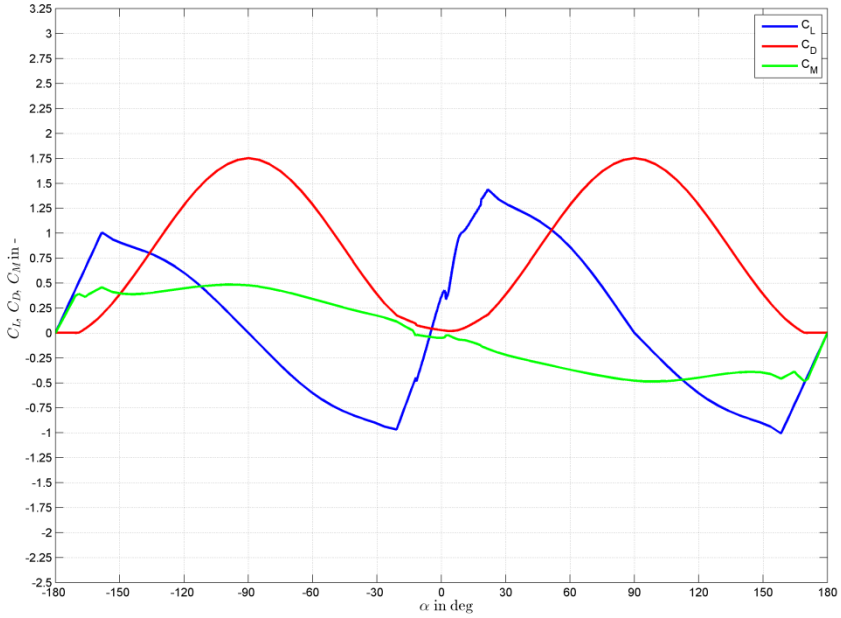

Figure B-15: Section 15 polars

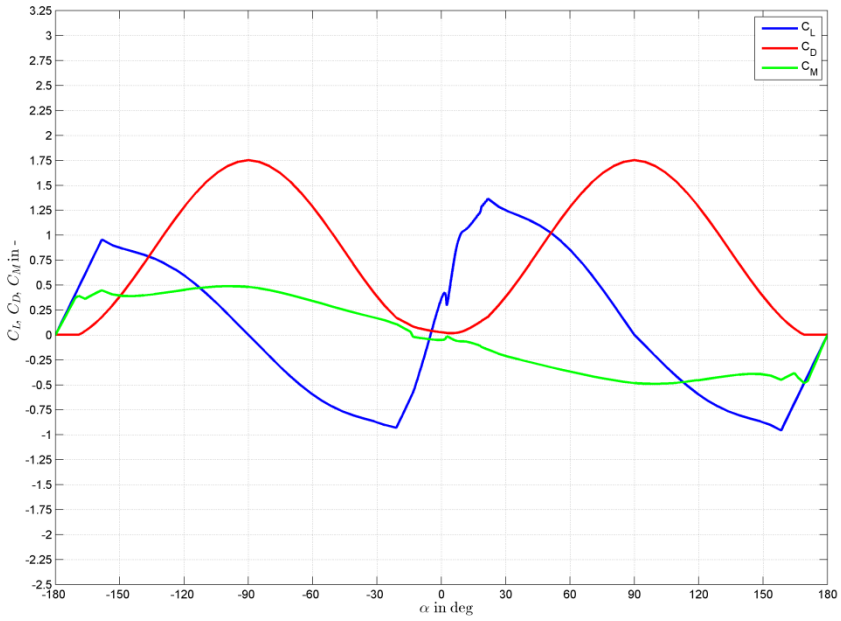

Figure B-16: Section 16 polars

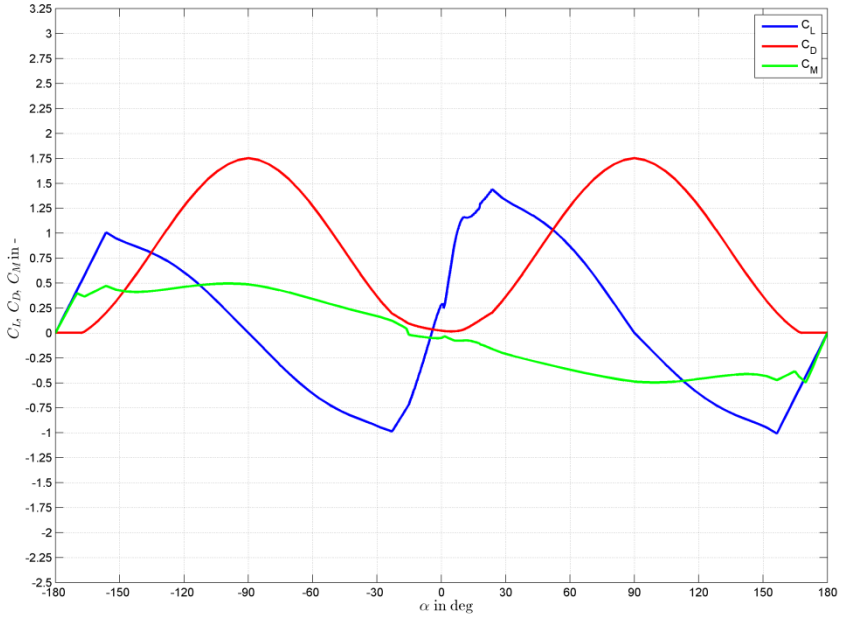

Figure B-17: Section 17 polars

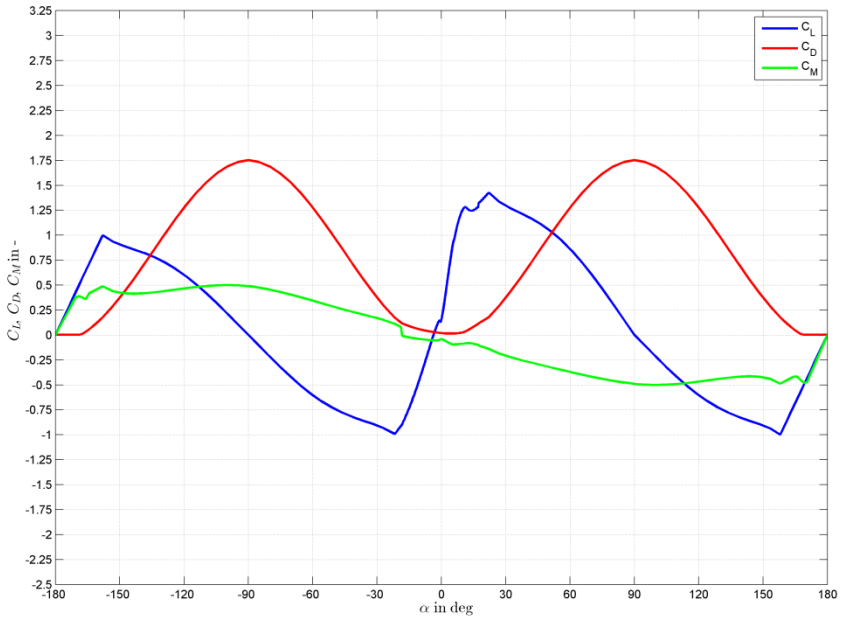

Figure B-18: Section 18 polars

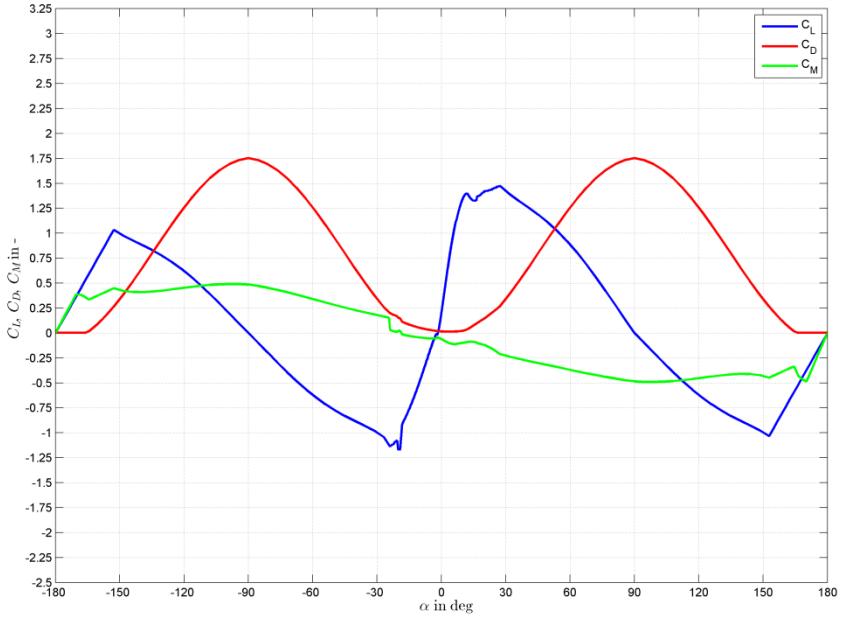

Figure B-19: Section 19 polars

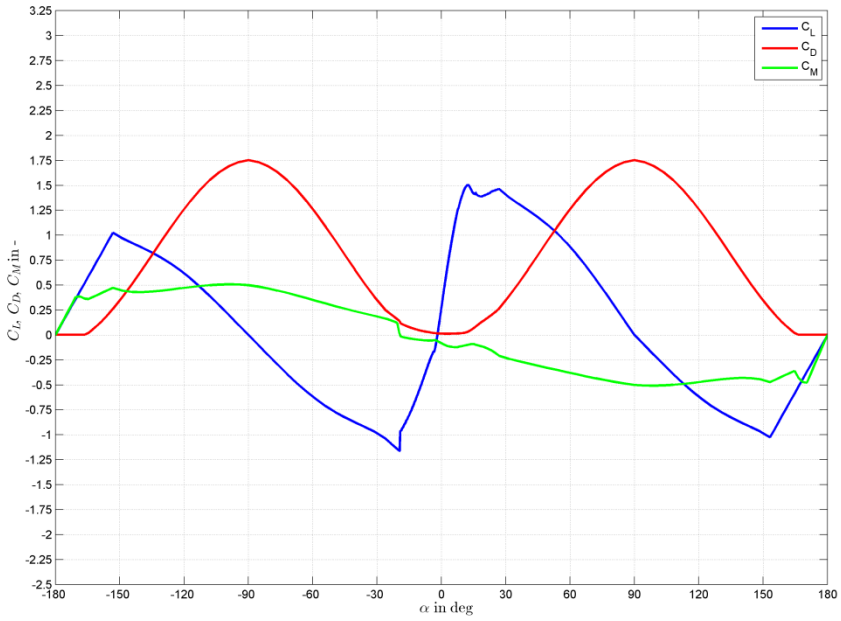

Figure B-20: Section 20 polars

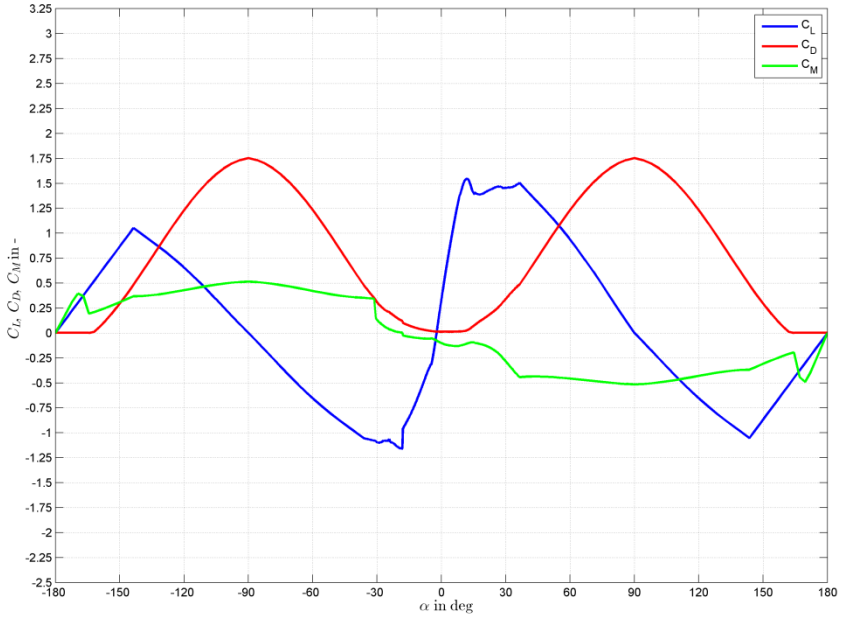

Figure B-21: Section 21 polars

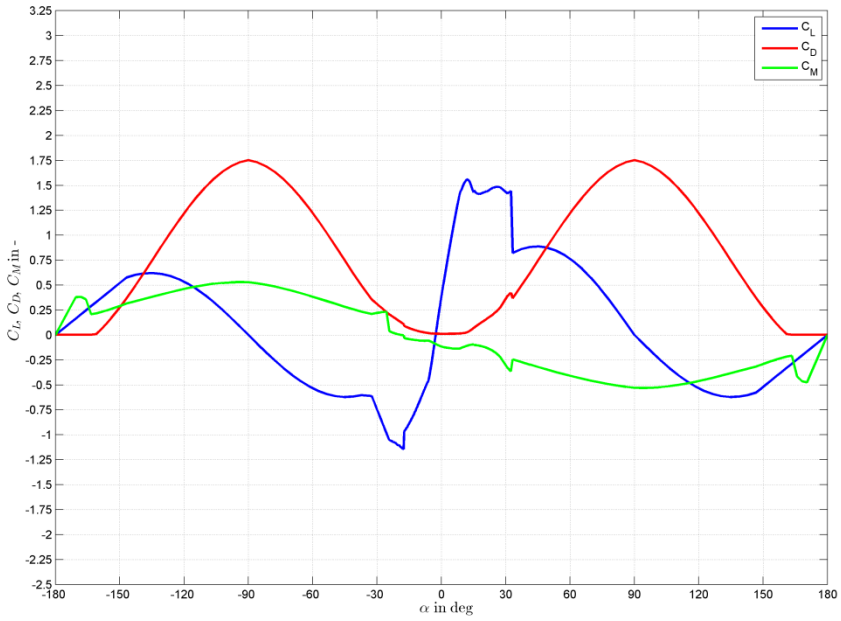

Figure B-22: Section 22 polars

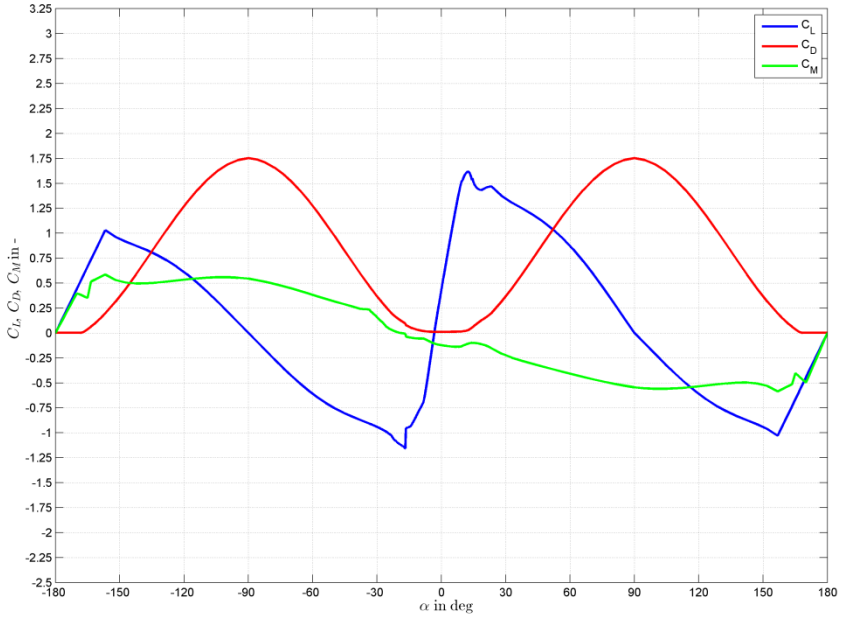

Figure B-23: Section 23 polars

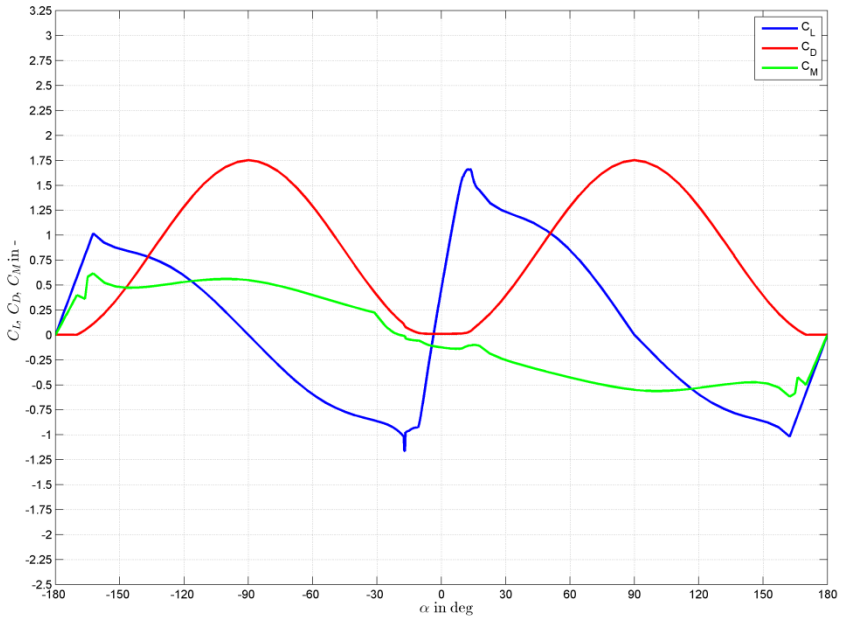

Figure B-24: Section 24 polars

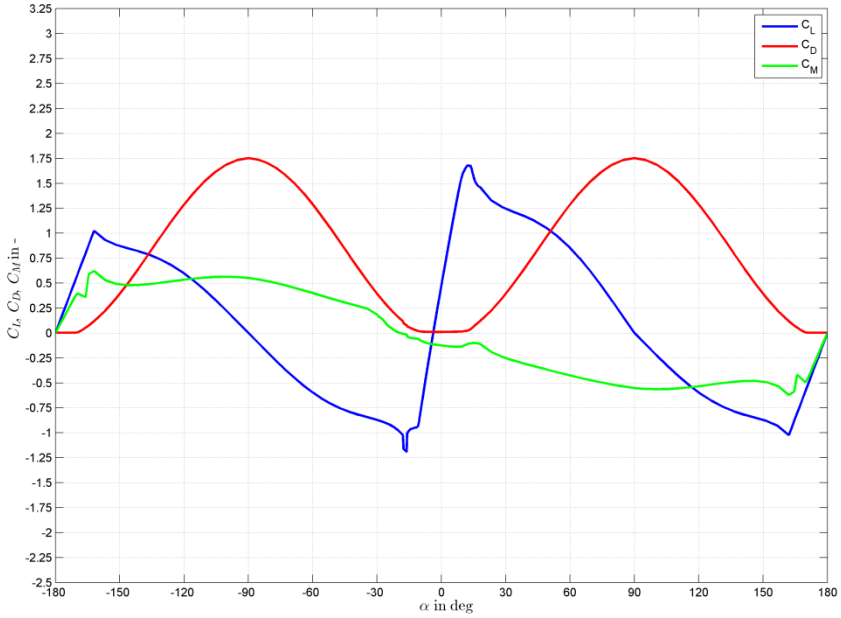

Figure B-25: Section 25 polars

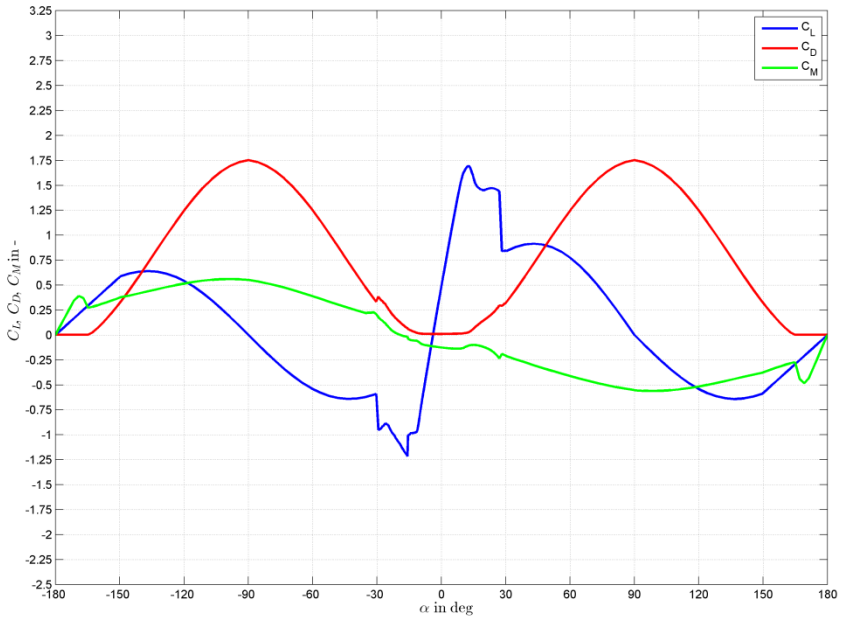

Figure B-26: Section 26 polars

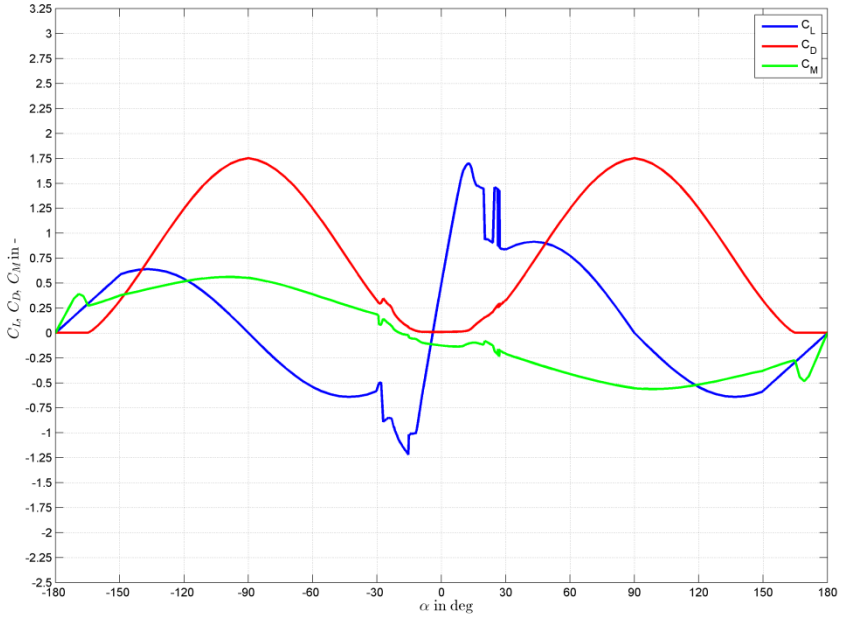

Figure B-27: Section 27 polars

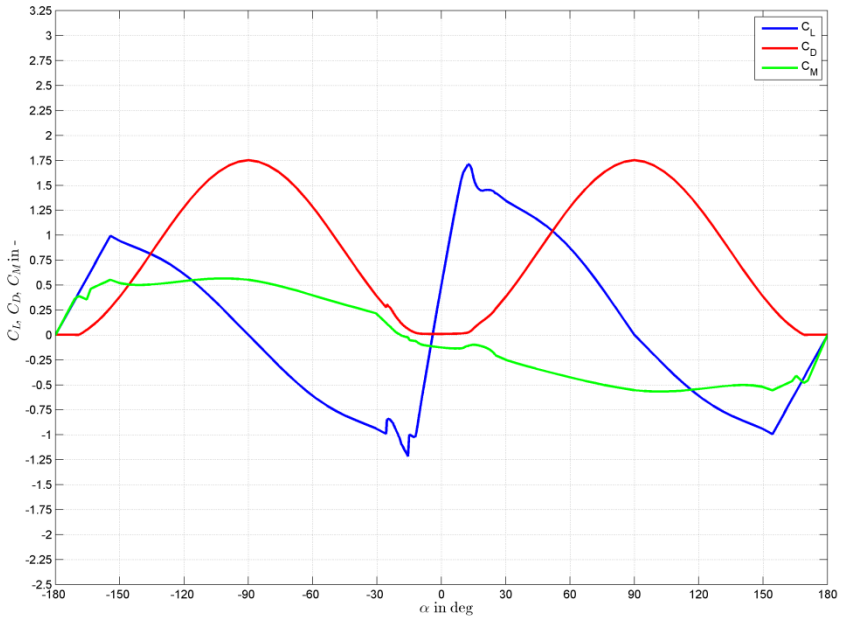

Figure B-28: Section 28 polars

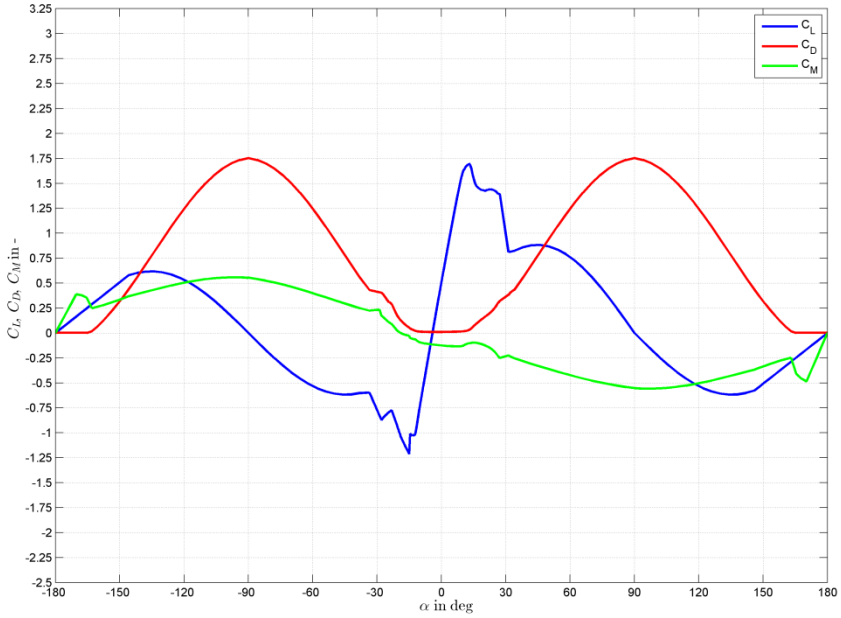

Figure B-29: Section 29 polars

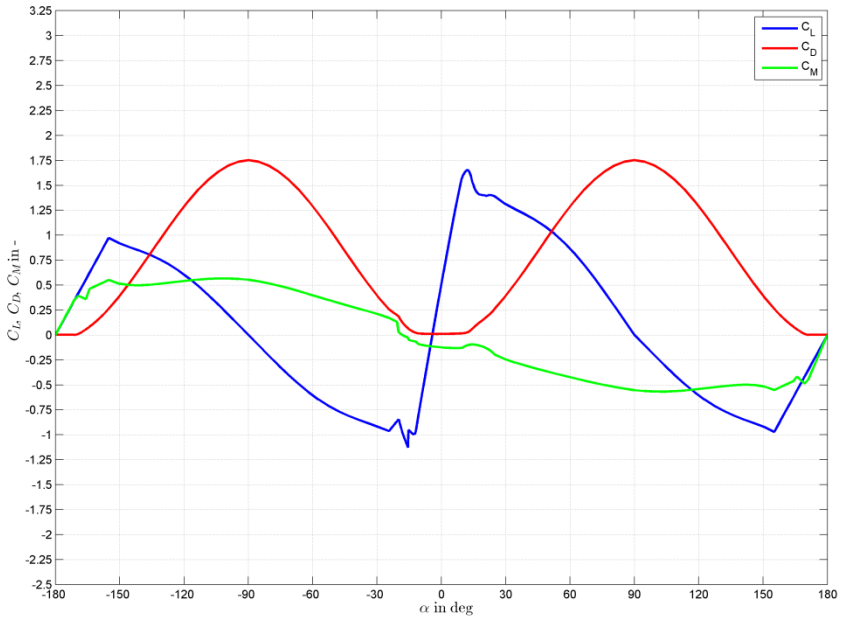

Figure B-30: Section 30 polars

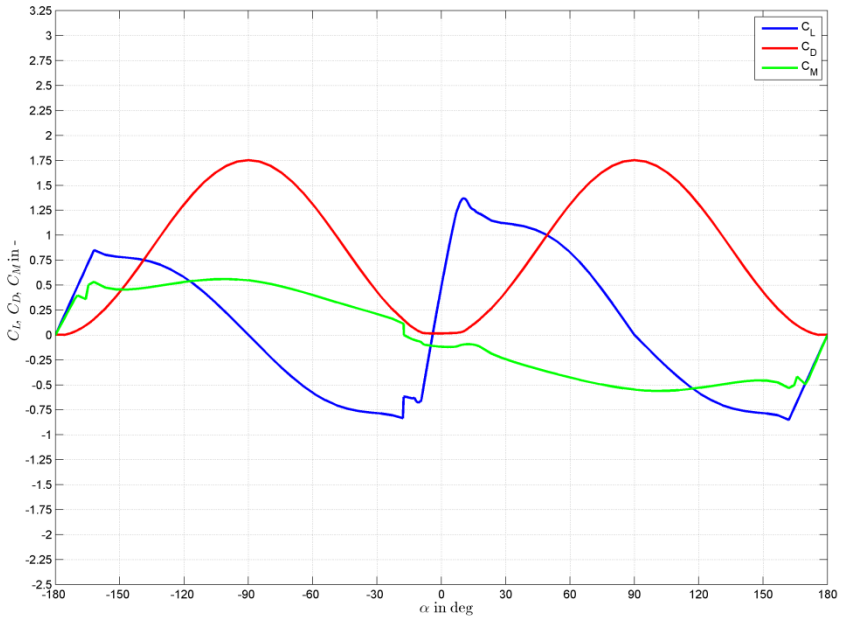

Figure B-31: Section 31 polars

Bibliography

[1] J. Jonkmann, S. Butterfield, W. Musial and G. Scott, "Definition of a 5-MW reference wind turbine for offshore system development," National Renewable Energy Laboratory, Golden, CO, 2009.

[2] C. Bak, F. Zahle, R. Bitsche, T. Kim, A. Yde, L. C. Henriksen, M. H. Hansen, J. P. A. A. Blasques, M. Gaunaa and A. Natarajan, "The DTU 10-MW reference wind turbine," Technical University of Denmark, Roskilde, 2013.

[3] IEC, "IEC 61400-1 Edition 3 – Wind turbines – Part 1: Design requirements," IEC, Geneva, 2005.

[4] Multibrid Entwicklungsgesellschaft mbh, "Pressemitteilung Errichtung Multibrid m5000," Multibrid Entwicklungsgesellschaft mbh, Bremerhaven, 2004.

[5] T. J. Larsen and A. M. Hansen, "How 2 HAWC2, the user's manual," Technical University of Denmark, Roskilde, 2015.

[6] J. P. A. A. Blasques, "User's Manual for BECAS: A cross section analysis tool for anisotropic and inhomogeneous beam sections of arbitrary geometry," Technical University of Denmark, Roskilde, 2012.

[7] W. A. Timmer and R. P. J. O. M. van Rooij, "Summary of the Delft University wind turbine dedicated airfoils," *Journal of Solar Energy Engineering,* vol. 125, no. 4, p. 488–496, November 2003.

[8] R. P. J. O. M. van Rooij, "Thick airfoile design," UpWind project, Delft, 2013.

[9] M. H. Hansen and L. C. Henriksen, "Basic DTU wind energy controller," Technical University of Denmark, Roskilde, 2013.

[10] E. A. Bossanyi and D. Witcher, "Controller for 5MW reference turbine," Garrad Hassan and Partners Limited, Bristol, 2009.

[11] E. A. Bossanyi, "Individual blade pitch control for load reduction," *Wind Energy,* vol. 6, no. 2, p. 119–128, April/June 2003.

[12] B. O. G. Montgomerie Jensen, A. J. Brand, J. Bosschiers and R. P. J. O. M. Van Rooji, "Three-dimensional effects in stall," Petten, 1997.

[13] M. Drela, "XFOIL: An analysis and design system for low Reynolds number airfoils," in *Low Reynolds Number Aerodynamics*, vol. 54, T. J. Mueller, Ed., Notre Dame, IN, Springer Berlin Heidelberg, 1989, p. 1–12.